

The Hidden Sterile Neutrino and the (2+2) Sum Rule

Heinrich Päs,¹ * Ligu Song,² † and Thomas J. Weiler² ‡

¹ *Institut für Theoretische Physik und Astrophysik, Universität Würzburg,
Am Hubland, 97074 Würzburg, Germany*

² *Department of Physics and Astronomy, Vanderbilt University
Nashville, TN 37235, USA*

Abstract

We discuss oscillations of atmospheric and solar neutrinos into sterile neutrinos in the 2+2 scheme. A zeroth order sum rule requires equal probabilities for oscillation into ν_s and ν_τ in the solar+atmospheric data sample. Data does not favor this claim. Here we use scatter plots to assess corrections of the zeroth order sum rule when (i) the 4×4 neutrino mixing matrix assumes its full range of allowed values, and (ii) matter effects are included. We also introduce a related “product rule”. We find that the sum rule is significantly relaxed, due to both the inclusion of the small mixing angles (which provide a short-baseline contribution) and to matter effects. The product rule is also dramatically altered. The observed relaxation of the sum rule weakens the case against the 2+2 model and the sterile neutrino. To invalidate the 2+2 model, a global fit to data *with the small mixing angles included* seems to be required.

*E-mail: paes@physik.uni-wuerzburg.de

†E-mail: liguo.song@vanderbilt.edu

‡E-mail: tom.weiler@vanderbilt.edu

I. INTRODUCTION

Taken at face value, the solar, atmospheric, and LSND data require three independent δm^2 scales. Thus, four neutrinos seem to be required. The Z -boson width further requires that one of these four neutrinos be a “sterile” $SU(2) \times U(1)$ electroweak-singlet. Given the profound theoretical implication which would accompany the validation of a light sterile neutrino, and given the present experimental search for the sterile neutrino by the mini-BooNE experiment [1], a serious look at the present viability of the sterile neutrino is well motivated.

It was shown some time ago that the non-observation of ν_e and ν_μ disappearance by the Bugey and CDHS experiments, in conjunction with the appearance of $\nu_\mu \rightarrow \nu_e$ in the LSND experiment, strongly disfavored the 3+1 spectral hierarchy [2,3] in which the large “LSND” mass-splitting isolates one heavier mass eigenstate $|\nu_H\rangle$ from the other three. The conflict results because the Bugey and CDHS rates are proportional to $|\langle \nu_e | \nu_H \rangle|^2$ and $|\langle \nu_\mu | \nu_H \rangle|^2$, respectively, whereas the LSND rate is proportional to the product of the two; the upper limits from Bugey and CDHS doubly-suppress the rate allowed for LSND. However, when the final value of the LSND oscillation amplitude was reported to be smaller [4] than earlier results, the 3+1 spectrum was resurrected at the 95% confidence limit for four isolated values of δm^2 [5–7]. Recently, a careful analysis of all data has led to the conclusion that even these isolated mass values are “highly unlikely,” viable only if one super-conservatively accepts the tiny intersections of the 99% Bugey/CDHS exclusion curve with the 99% allowed region of LSND [8]. This 3+1 spectrum is a “separated-sterile” model, in that the sterile flavor resides dominantly in the isolated mass-state and barely mixes with the three active flavors; in the absence of the LSND data, the active-sterile mixing can be made arbitrarily small.

On the other hand, the alternative 2+2 mass spectrum is compatible with the combination of short baseline data. In the 2+2 spectrum, the LSND scale splits two pairs of neutrino mass-eigenstates. Phenomenologically, it is required that one pair mix ν_μ with ν_τ and ν_s to explain the atmospheric ν_μ disappearance, while the second pair mix ν_e with ν_τ and ν_s to explain the solar ν_e disappearance. The small LSND amplitude, and the Bugey and CDHS limits are accommodated with a small mixing of ν_e into the first pair, and small

mixing of ν_μ into the second pair [3]. In this model, the sterile neutrino is distributed in its totality between the solar and atmospheric scales. This leads to an approximate sum rule [9]. The essence of the sum rule is that the sterile neutrino may hide from solar oscillations, or from atmospheric oscillations, but cannot hide from both. When matter effects and small angles mixing the atmospheric and solar pairs are neglected, the sum rule states that the probabilities to produce ν_s in the solar and atmospheric data sum to unity.

The Superkamiokande (SK) experiment has put a limit on the atmospheric mode $\nu_\mu \rightarrow \nu_s$ [10]. In principle, the atmospheric data is sensitive to sterile neutrinos in three ways: (i) through differing matter effects for ν_μ oscillation to ν_τ vs. ν_s ; (ii) through neutral current scattering of ν_τ but not ν_s , as measured by π^0 production; and (iii) through τ appearance from ν_τ scattering above threshold. However, the SuperK analysis, following the guidelines in [11], ignores all parameters but δm_{atm}^2 , θ_{atm} , and the ν_τ - ν_s mixing angle $\theta_{\tau s}$. We will argue that the short baseline contribution from the large mass-gap δm_{LSND}^2 is important if the small mixing angles are not too small, in which case the SuperK analysis is invalid for the 2+2 model.

Limits on the solar mode $\nu_e \rightarrow \nu_s$ result from model fits to the SK solar data [12], but especially from the recent SNO data. There is no evidence favoring a sterile admixture in the neutrino flux from the sun. Nevertheless, a large sterile component remains compatible with the SNO result [13,14], because of our uncertainty in the true high-energy solar neutrino flux produced by the ^8B reaction in the sun. It is unclear whether future measurements of intermediate-energy neutrinos in the BOREXINO experiment or the solar neutrino component of the KAMLAND experiment will help resolve this issue.

Combined fits to solar and atmospheric neutrinos [15–17] have been performed. The authors of [16] came recently to the conclusion that a global analysis considering short baseline, solar, and atmospheric data gives a slightly better fit to (3+1) mass schemes compared to (2+2) schemes, though both four-neutrinos schemes are presently viable at low confidence. Most recently, a global analysis [17] has been performed which includes the LSND data, and newest SNO, SuperK, and MACRO data. The conclusion reached is that both the 2+2 and 1+3 sterile models are highly disfavored; the 2+2 analysis returns a goodness of fit of only 1.6×10^{-6} . However, to reduce the number of parameters involved,

these papers set the two smallest mixing angles tested by short baseline experiments to zero in their fits to the solar and atmospheric data.

In this work, we analyze the approximate sum rule in generality, varying the usually neglected mixing angles in their experimentally allowed ranges, and including possible matter effects. Our results indicate the allowed range of joint probability for ν_s to reside in the solar and atmospheric data. We find that the allowed range may differ considerably from the zeroth order result with small mixing-angles set to zero. Although it is not known whether the same values of the small angles which provide a large violation of the zeroth order sum rule also provide good fits to the global data, the sensitivity to small mixing-angles demonstrated here suggests that global fits which neglect the small angles may underestimate the viability of the 2+2 model. This, in turn, casts some doubt on claimed exclusions of the 2+2 model. The ultimate arbiter on the viability of the sterile neutrino will be a global fit to data with all mixing angles included.¹

II. FORMALISM

The starting point for neutrino oscillations is the unitary transformation between mass and flavor basis:

$$|\nu_\alpha\rangle = \sum_j U_{\alpha j}^* |\nu_j\rangle, \quad \text{or} \quad \langle \nu_j | \nu_\alpha \rangle = (U^\dagger)_{j\alpha}; \quad (1)$$

the inverse relation is

$$|\nu_j\rangle = \sum_\alpha (U^\dagger)_{j\alpha}^* |\nu_\alpha\rangle, \quad \text{or} \quad \langle \nu_\alpha | \nu_j \rangle = U_{\alpha j}. \quad (2)$$

We will consistently use roman indices for mass states, and greek indices for flavor states. The mass states $|\nu_j\rangle$ and therefore the transformation matrix U depend on matter densities, and so we will often affix a superscript or subscript label $\kappa \in \{V, S, M, C\}$ to $|\nu_j\rangle$ and U

¹Of the three small angles, we show that the sum rule is sensitive to $\epsilon_{\mu\mu}$ and $\epsilon_{\mu e}$, but not to ϵ_{ee} (in our notation). $\epsilon_{\mu\mu}$ has been included in recent global analyses. Our findings suggest that, at a minimum, $\epsilon_{\mu e}$ should be included too.

to signify the vacuum, solar, earth's mantle, and earth's core environments, respectively. In addition, the labels A and E will sometimes denote the atmosphere and the Earth.

The formula for the oscillation probability is

$$P^{\alpha \rightarrow \beta} = \delta_{\alpha\beta} - 4 \sum_{j < k} \left[R_{\beta k}^{\alpha j} \sin^2(\Phi_{kj}) + \frac{1}{2} J_{\beta k}^{\alpha j} \sin(2\Phi_{kj}) \right], \quad (3)$$

where the CP-conserving coefficient $R_{\beta k}^{\alpha j}$ and the CP-violating coefficient $J_{\beta k}^{\alpha j}$ are the real and imaginary parts, respectively, of $U_{\alpha j} U_{\beta j}^* U_{\alpha k}^* U_{\beta k}$, and the relative phase $\Phi_{kj} \equiv \delta m_{kj}^2 L / 4E = 1.27 (\delta m_{kj}^2 / \text{eV}^2) (L / \text{km}) / (E / \text{GeV})$, with $\delta m_{kj}^2 = m_k^2 - m_j^2$. The oscillation length, determined by setting $\Phi_{kj} = \pi$, is

$$\lambda = 2.48 \left(\frac{\text{eV}^2}{\delta m_{kj}^2} \right) \left(\frac{E}{\text{GeV}} \right) \text{ km}. \quad (4)$$

This same probability formula holds in vacuum or in matter at near-constant density, although the mixing elements and the effective masses differ in these two situations.

After many oscillations, the coherence implied by the specific phases in eq. (3) is lost, due to magnification of experimental uncertainties in L/E or due to decoherence of the mass-eigenstate wave packets. For either reason, the result is an averaging which takes $\sin^2(\Phi_{kj}) \rightarrow \frac{1}{2}$ and $\sin(2\Phi_{kj}) \rightarrow 0$. This same averaging occurs also after even a few oscillations if the experimental uncertainties in L/E are sufficiently large. It is also important to note that the increase of λ with E may lead to the suppression of oscillations at high energy, if the condition $\lambda \gg L$ is achieved. This suppression, together with matter effects, will become important in the discussion of through-going atmospheric neutrino events.

Four-flavor mixing is described by six angles and three CP-violating phases. In addition there are three further phases for Majorana neutrinos; since these three phases do not enter into oscillation probabilities, we omit them. The six angles parametrize independent rotations in the six planes of four-dimensional space. For our purposes, it is useful to order these rotations as²

$$U = R_{23}(\theta_{\tau s}) R_{24}(\epsilon_{\mu\mu}) R_{14}(\epsilon_{\mu e}) R_{13}(\epsilon_{ee}) R_{34}(\theta_{\text{atm}}) R_{12}(\theta_{\text{sun}}). \quad (5)$$

²We note that the ordering in eq. (5) is the same as that in [15–17] when $\epsilon_{\mu e}$ and ϵ_{ee} are set to zero, as is done in [15–17].

Unitary U transforms from the mass basis (m_4, m_3, m_2, m_1) to the flavor basis $(\nu_\mu, \nu_\tau, \nu_s, \nu_e)$. In suggestive notation, the ϵ 's are small angles limited by the short-baseline (SBL) data, θ_{sun} and θ_{atm} are the angles dominantly responsible for solar and atmospheric oscillations, respectively, and $\theta_{\tau s}$ is a possibly large angle parametrizing the dominant mixing of the ν_τ and ν_s flavors. Explicitly, the ν_τ - ν_s mixing resulting from $R_{23}^T(\theta_{\tau s})$ is

$$\begin{pmatrix} \nu_+ \\ \nu_- \end{pmatrix} = \begin{pmatrix} \cos \theta_{\tau s} & -\sin \theta_{\tau s} \\ \sin \theta_{\tau s} & \cos \theta_{\tau s} \end{pmatrix} \begin{pmatrix} \nu_\tau \\ \nu_s \end{pmatrix}. \quad (6)$$

As shown in [18], the three phases may be assigned to the double-generation skipping rotations R_{24} and R_{13} and any one of the single-generation skipping rotations, in the following manner: equal and opposite phases are attached to the two non-diagonal elements of the rotation matrix. For the single-generation skipping complex rotation, we choose R_{14} . Since the three angles of R_{24} , R_{13} , and R_{14} are small, this amounts to assigning an arbitrary phase to each of the $\sin(\epsilon_j) \sim \epsilon_j$'s, with ϵ_j to the right of the diagonal and ϵ_j^* to the left.³ The small-angle part of U is then $U_\epsilon \equiv R_{24}(\epsilon_{\mu\mu})R_{14}(\epsilon_{\mu e})R_{13}(\epsilon_{ee})$, which to order ϵ^2 is

$$U_\epsilon = \begin{pmatrix} 1 - \frac{1}{2}(|\epsilon_{\mu\mu}|^2 + |\epsilon_{\mu e}|^2) & -\epsilon_{ee}^* \epsilon_{\mu e} & \epsilon_{\mu\mu} & \epsilon_{\mu e} \\ 0 & 1 - \frac{1}{2}|\epsilon_{ee}|^2 & 0 & \epsilon_{ee} \\ -\epsilon_{\mu\mu}^* & 0 & 1 - \frac{1}{2}|\epsilon_{\mu\mu}|^2 & -\epsilon_{\mu\mu}^* \epsilon_{\mu e} \\ -\epsilon_{\mu e}^* & -\epsilon_{ee}^* & 0 & 1 - \frac{1}{2}(|\epsilon_{ee}|^2 + |\epsilon_{\mu e}|^2) \end{pmatrix}. \quad (7)$$

We note that with this parameterization the nonzero phases are associated exclusively with small angles, making the smallness of any observable CP-violation in the 2+2 scheme immediately evident.

When the CP-violating phases are allowed to range from 0 to π , all angles may be restricted to the interval $[0, \pi/2]$. However, when the phases are neglected, the θ 's still range over $[0, \pi/2]$, but the ϵ 's now range over $[-\pi/2, \pi/2]$ (or over $[0, \pi]$).

The two large-angle mixings on the right in eq. (5) are given by

³The small-angle expansion of $\cos(\epsilon_j)$ is $1 - \frac{1}{2}|\epsilon_j|^2$.

$$U_{\pm} = R_{34}(\theta_{\text{atm}})R_{12}(\theta_{\text{sun}}) = \begin{pmatrix} \cos \theta_{\text{atm}} & \sin \theta_{\text{atm}} & 0 & 0 \\ -\sin \theta_{\text{atm}} & \cos \theta_{\text{atm}} & 0 & 0 \\ 0 & 0 & \cos \theta_{\text{sun}} & \sin \theta_{\text{sun}} \\ 0 & 0 & -\sin \theta_{\text{sun}} & \cos \theta_{\text{sun}} \end{pmatrix}. \quad (8)$$

This matrix independently mixes each of the two mass doublets in the 2+2 spectrum. U_{\pm} approximates the full mixing matrix in the $(\nu_{\mu}, \nu_{+}, \nu_{-}, \nu_e)$ basis. The advantage of locating U_e to the left of U_{\pm} is that in the full mixing matrix U , the angle θ_{atm} appears only in the first two columns, and θ_{sun} appears only in the last two columns. Consequently, atm/LBL amplitudes do not depend on θ_{sun} , and solar amplitudes do not depend on θ_{atm} . Of course, in any parameterization, the SBL amplitudes are insensitive to mixing within either mass doublet, and so depend on neither θ_{atm} nor on θ_{sun} .

Recent global fits of the 2+2 model to solar and atmospheric data [15–17] have focused on the seven-parameter set $\{\epsilon_{\mu\mu}, \theta_{\tau s}, \theta_{\text{sun}}, \theta_{\text{atm}}, \delta m_{\text{LSND}}^2, \delta m_{\text{sun}}^2, \delta m_{\text{atm}}^2\}$, neglecting the two small angles $\epsilon_{\mu e}, \epsilon_{ee}$, and the three CP-violating phases.⁴ The investigation of the dependence of the sterile neutrino sum rule on the small angles (ϵ 's) in this paper suggests that neglect of these small angles, especially $\epsilon_{\mu e}$, may not be warranted.

III. SUM AND PRODUCT RULES

A. Zeroth order in ϵ 's

Let us first discuss the oscillation probabilities in vacuum in the limit where the ϵ 's are set to zero. This limit results when $\langle \nu_e | \nu_4 \rangle = 0 = \langle \nu_e | \nu_3 \rangle$, and $\langle \nu_{\mu} | \nu_2 \rangle = 0 = \langle \nu_{\mu} | \nu_1 \rangle$.

In the limit of vanishing ϵ 's, one can use eq. (8) to read off immediately that LBL/atm oscillations of the ν_e are zero and ν_{μ} oscillates into pure ν_{+} ; at the solar-scale, $\nu_e \rightarrow \nu_{\mu}$ oscillations are zero, and ν_e oscillates into pure ν_{-} ; and there are no SBL oscillations.

It proves useful to denote the amplitude of the CP-conserving oscillation at each δm^2 scale (short-baseline/LSND, long-baseline/atmospheric, and solar) by [3]

⁴In ref. [17] the angles $\epsilon_{\mu e}$ and ϵ_{ee} are turned on, but only in the LSND part of the analysis.

$$A_{\text{SBL}}(\nu_\alpha \rightarrow \nu_\beta) = -4 \sum_{j=1}^2 \sum_{k=3}^4 R_{\beta k}^{\alpha j}; \quad A_{\text{LBL}}(\nu_\alpha \rightarrow \nu_\beta) = -4R_{\beta 4}^{\alpha 3}; \quad A_{\text{sun}}(\nu_\alpha \rightarrow \nu_\beta) = -4R_{\beta 2}^{\alpha 1}. \quad (9)$$

The disappearance amplitude is denoted by

$$A_\Delta(\nu_\beta \rightarrow \nu_\beta) = \sum_{\alpha \neq \beta} A_\Delta(\nu_\beta \rightarrow \nu_\alpha) = 4 \sum_\Delta |U_{\beta j}|^2 |U_{\beta k}|^2; \quad (10)$$

here, Δ denotes the SBL, LBL/atm, or solar scale, and \sum_Δ denotes the sum over the appropriate mass states indicated explicitly in eq. (9). Similarly, the CP-conserving contribution to the probability at each δm^2 scale is denoted by

$$P_\Delta(\nu_\alpha \rightarrow \nu_\beta) \equiv A_\Delta(\nu_\alpha \rightarrow \nu_\beta) \sin^2 \left(\frac{\delta m_\Delta^2 L}{4E} \right). \quad (11)$$

Some care is required in applying these contributions to oscillation data, since observables at any given scale will in general receive contributions from that scale and all shorter scales. Such is not the case with the block-diagonal mixing of eq. (8).

Explicitly, the nonzero oscillation amplitudes for ν_μ due to atmospheric-scale oscillations are

$$A_{\text{atm}}(\nu_\mu \rightarrow \nu_\tau) = \sin^2(2\theta_{\text{atm}}) \cos^2 \theta_{\tau s} \quad (12)$$

$$A_{\text{atm}}(\nu_\mu \rightarrow \nu_s) = \sin^2(2\theta_{\text{atm}}) \sin^2 \theta_{\tau s} \quad (13)$$

$$A_{\text{atm}}(\nu_\mu \rightarrow \nu_\mu) = \sin^2(2\theta_{\text{atm}}) \quad (14)$$

while for ν_e due to solar-scale oscillations they are

$$A_{\text{sun}}(\nu_e \rightarrow \nu_\tau) = \sin^2(2\theta_{\text{sun}}) \sin^2 \theta_{\tau s} \quad (15)$$

$$A_{\text{sun}}(\nu_e \rightarrow \nu_s) = \sin^2(2\theta_{\text{sun}}) \cos^2 \theta_{\tau s} \quad (16)$$

$$A_{\text{sun}}(\nu_e \rightarrow \nu_\mu) = \sin^2(2\theta_{\text{sun}}) \quad (17)$$

We note that matter effects cannot alter the texture of the off-diagonal elements of the mass-squared matrix in the flavor basis, because the matter potential is diagonal in this basis. Consequently, the block-diagonal structure of the diagonalizing matrix in eq. (8) is maintained in the presence of matter. This further implies that eqs. (12) to (16) are

unchanged in form by matter, although the angles (and mass-eigenvalues) assume different values.

In solar matter, there is an essential nuance enriching the neutrino physics: The evolution of the neutrinos from the sun's center to the sun's surface is dominated by matter effects. The solar matter-density is not constant, and so the matter-dependent mixing-angles change continuously as the neutrinos transit the sun, possibly effecting non-adiabatic transitions among mass-eigenstates. However, for large θ_{sun} , which holds for the LMA solution which we consider in this work (and for the QVO and VO solutions), the neutrino propagates adiabatically from the sun's center to the surface. This means that the neutrino emerges into vacuum with the combination of mass eigenstates unchanged from that determined at the sun's center. Moreover, solar neutrinos with energies above the solar resonance associated with δm_{sun}^2 and below the atmospheric resonance associated with δm_{atm}^2 will evolve adiabatically to emerge from the sun in a nearly pure ν_2 mass-eigenstate. The solar and atmospheric resonant energies in the 2+2 model in the zero ϵ 's approximation are [19]

$$E_{\odot}^R \approx \frac{\delta m_{\text{sun}}^2 \cos(2\theta_{\text{sun}})}{2(A_{CC} - \cos^2(\theta_{\tau s})A_{NC})}, \quad (18)$$

and

$$E_{\text{atm}}^R \approx \frac{\delta m_{\text{atm}}^2 \cos(2\theta_{\text{atm}})}{2 \sin^2(\theta_{\tau s})A_{NC}}, \quad (19)$$

respectively. The vacuum angles and mass-squared differences are defined previously, and $A_{CC} = \sqrt{2}G_F N_e$ and $A_{NC} \approx \frac{1}{2}A_{CC}$ are the effective contributions of the matter potential to the Hamiltonian in the flavor basis, written in terms of the electron number density. Putting in the values $N_e(0) = 6.0 \times 10^{25} \text{cm}^{-3}$ for the electron density at the center of the sun, $\delta m_{\text{sun}}^2 = 4 \times 10^{-5} \text{eV}^2$, and $\delta m_{\text{atm}}^2 = 3 \times 10^{-3} \text{eV}^2$, one finds adiabatic evolution to near-pure ν_2 for large-angle solar mixing and energies in the range between $E_{\odot}^R = 4 \cos(2\theta_{\text{sun}})(1 + \sin^2 \theta_{\tau s})^{-1} \text{MeV}$ and $E_{\text{atm}}^R = 300 \cos(2\theta_{\text{atm}})(\sin^2 \theta_{\tau s})^{-1} \text{MeV}$. The solar neutrinos from the ${}^8\text{B}$ decay chain, measured in the SuperK and SNO experiments, lie within this energy range.

The neutrinos arriving at earth from the sun are incoherent mass eigenstates.⁵ Thus,

⁵Even if the neutrinos exiting the sun bear coherent phase relationships, they decohere in transit

the density operator describing the decoherent ensemble of neutrinos arriving at earth from the sun is diagonal in the mass basis. In the adiabatic approximation, it is simply

$$\hat{\rho}_{\text{mass}}^S = \sum_j |U_{ej}^S|^2 |\nu_j\rangle\langle\nu_j|. \quad (20)$$

Here, U^S is the mixing matrix at the center of the sun where the solar neutrinos originate. Let us label the solar neutrino “ ν_\odot ” to signify its $\nu_e \rightarrow \nu_{SUN}$ solar history. The probability to measure neutrino flavor β at earth is then given by

$$P_S(\nu_\odot \rightarrow \nu_\beta) = \langle \nu_\beta | \hat{\rho}^S | \nu_\odot \rangle = \sum_j |U_{ej}^S|^2 |U_{\beta j}^V|^2, \quad (21)$$

after applying eqs. (1) and (2). The $\nu_\odot \equiv \nu_2$ approximation⁶ consists of setting $|U_{ej}^S|^2$ equal to δ_{j2} , yielding

$$P_{\nu_\odot \rightarrow \nu_\beta} = |U_{\beta 2}^V|^2 \quad [\nu_\odot \equiv \nu_2, \text{adiabatic}] \quad (22)$$

In the absence of ϵ 's, we have from eqs. (6), (8), and (22), that

$$\nu_2 = \cos\theta_{\text{sun}}(\sin\theta_{\tau s}\nu_\tau + \cos\theta_{\tau s}\nu_s) - \sin\theta_{\text{sun}}\nu_e. \quad (23)$$

From this equation, we may read off the values of $U_{\beta 2}^V$ to obtain the oscillation amplitudes for solar neutrinos arriving at the earth in the $\nu_\odot \equiv \nu_2$ approximation:

$$A_{\text{sun}}(\nu_\odot \rightarrow \nu_\tau) = \cos^2(\theta_{\text{sun}}) \sin^2\theta_{\tau s} \quad (24)$$

$$A_{\text{sun}}(\nu_\odot \rightarrow \nu_s) = \cos^2(\theta_{\text{sun}}) \cos^2\theta_{\tau s} \quad (25)$$

$$A_{\text{sun}}(\nu_\odot \rightarrow \nu_e) = \cos^2(\theta_{\text{sun}}) \quad (26)$$

In these formulas, the angles are truly vacuum angles.

to Earth if $\delta m_{\text{sun}}^2 \gtrsim 10^{-10} \text{eV}^2$, due to the many oscillation lengths contained in the one A.U. path length.

⁶In our numerical work we will go beyond the $\nu_\odot \equiv \nu_2$ approximation. Nevertheless, $\nu_\odot \equiv \nu_2$ is a good approximation offering simple results. Numerically, we find that $|U_{e2}^S|^2 = 90\%$, 98% , and 99% for $E_\nu = 5, 10,$ and 15 MeV, respectively, for zero ϵ 's, and with little change for nonzero ϵ 's.

Thus, unitarity in the context of the 2+2 mass spectrum has led one to a sum rule [9] and a product rule at zeroth order in ϵ :

$$\left[\frac{P(\nu_{\odot} \rightarrow \nu_s)}{P(\nu_{\odot} \rightarrow \nu_{\ell})} \right]_{\text{sun}} + \left[\frac{P(\nu_{\mu} \rightarrow \nu_s)}{P(\nu_{\mu} \rightarrow \nu_{\mu})} \right]_{\text{atm}} = (\cos^2 \theta_{\tau s})_V + (\sin^2 \theta_{\tau s})_E \rightarrow 1 \quad (27)$$

and

$$\left[\frac{P(\nu_{\odot} \rightarrow \nu_s)}{P(\nu_{\odot} \rightarrow \nu_{\tau})} \right]_{\text{sun}} \times \left[\frac{P(\nu_{\mu} \rightarrow \nu_s)}{P(\nu_{\mu} \rightarrow \nu_{\tau})} \right]_{\text{atm}} = (\cot^2 \theta_{\tau s})_V \times (\tan^2 \theta_{\tau s})_E \rightarrow 1 \quad (28)$$

where the subscripts V and E signify “vacuum” and “earth-matter”, and the arrows hold in the limit of negligible earth-matter effects. In the figures to follow and the discussion thereof we will refer to the ratio terms in eqs (27) and (28) as R_{sun} and R_{atm} , respectively.

We emphasize that the sum and product rules are not required by any underlying symmetry or principle. Rather, they are accidents of the block-diagonal structure of eq. (8), which results when the small angles are neglected. The values on the right-hand sides of these two rules, eqs. (27) and (28), will differ from unity when the small mixing angles are included, even if matter-effects are absent. Furthermore, although their values are intimately related at zeroth order in the ϵ 's, they are not so simply related at higher order in ϵ 's.

The purpose of this paper is to evaluate these sum rules, including the small angles neglected in previous work, and including possible earth-matter effects. In the next section, we calculate oscillation probabilities to order ϵ^2 , to find the order ϵ^2 corrections to the sum (27) and product (28) rules. In section V we numerically evaluate the sum and product rules without approximation. Readers interested only in the answers may jump over the remaining formalism to find the results presented in section V.

B. Order ϵ and ϵ^2 corrections

To order ϵ^2 , the full mixing matrix in the physical flavor-basis $(\nu_{\mu}, \nu_{\tau}, \nu_s, \nu_e)$ is the product

$$U = \begin{pmatrix} 1 & 0 & 0 & 0 \\ 0 & \cos \theta_{\tau s} & \sin \theta_{\tau s} & 0 \\ 0 & -\sin \theta_{\tau s} & \cos \theta_{\tau s} & 0 \\ 0 & 0 & 0 & 1 \end{pmatrix} \times U_{\epsilon} \times U_{\pm} \quad (29)$$

where U_ϵ and U_\pm are given in eqs. (7) and (8). This mixing matrix determines all of the oscillation amplitudes to $\mathcal{O}(\epsilon^2)$, and so determines the $\mathcal{O}(\epsilon)$ and $\mathcal{O}(\epsilon^2)$ modifications to the sum rules. Here we give the individual flavor-changing amplitudes for SBL, solar, and atmospheric neutrinos to $\mathcal{O}(\epsilon^2)$. We begin with the SBL amplitudes, and summarize the existing experimental constraints on these amplitudes.

In our notation, the SBL oscillation amplitudes to order $|\epsilon|^2$ are

$$A_{\text{SBL}}(\nu_e \rightarrow \nu_\mu) = 4 [|\epsilon_{\mu e}|^2 + |\epsilon_{ee}|^2] \quad (30)$$

$$A_{\text{SBL}}(\nu_\mu \rightarrow \nu_\mu) = 4 [|\epsilon_{\mu e}|^2 + |\epsilon_{\mu\mu}|^2] \quad (31)$$

$$A_{\text{SBL}}(\nu_\mu \rightarrow \nu_e) = 4 |\epsilon_{\mu e}|^2 \quad (32)$$

$$A_{\text{SBL}}(\nu_\mu \rightarrow \nu_\tau) = 4 |\epsilon_{\mu\mu}|^2 \sin^2 \theta_{\tau s} \quad (33)$$

$$A_{\text{SBL}}(\nu_\mu \rightarrow \nu_s) = 4 |\epsilon_{\mu\mu}|^2 \cos^2 \theta_{\tau s} \quad (34)$$

$$A_{\text{SBL}}(\nu_e \rightarrow \nu_\tau) = 4 |\epsilon_{ee}|^2 \cos^2 \theta_{\tau s} \quad (35)$$

$$A_{\text{SBL}}(\nu_e \rightarrow \nu_s) = 4 |\epsilon_{ee}|^2 \sin^2 \theta_{\tau s}. \quad (36)$$

These amplitudes, and so the values of the small angles ϵ_{ee} , $\epsilon_{\mu e}$ and $\epsilon_{\mu\mu}$, are bounded from above by the experimental limits on ν_μ and ν_e disappearance in vacuum, and by atmospheric neutrino oscillation data. The positive result of LSND bounds $\epsilon_{\mu e}$ from below, but this constraint is not significant for present purposes. For the allowed LSND region $\delta m_{\text{SBL}}^2 \sim 1.0$ to 0.2 eV^2 , the BUGEY disappearance experiment [21] provides the 90 % C.L. bound⁷ $\frac{1}{4}A_{\text{SBL}}(\nu_e \rightarrow \nu_\mu) = |\epsilon_{ee}|^2 + |\epsilon_{\mu e}|^2 \leq 0.01$. The CDHS [22] $\bar{\nu}_\mu$ (ν_μ) disappearance experiment bounds the amplitude $\frac{1}{4}A_{\text{SBL}}(\nu_\mu \rightarrow \nu_\mu) = |\epsilon_{\mu\mu}|^2 + |\epsilon_{\mu e}|^2 \leq 0.2$ for $\delta m_{\text{SBL}}^2 \gtrsim 0.3 \text{ eV}^2$. In fact, a more stringent bound on $A_{\text{SBL}}(\nu_\mu \rightarrow \nu_\mu)$ results from atmospheric neutrino data (a nonzero value for this amplitude is incompatible with maximal ν_μ mixing at the δm_{atm}^2 scale). A fit to atmospheric data [15] results in $A_{\text{SBL}}(\nu_\mu \rightarrow \nu_\mu) < 0.48$ (0.64) with 90% (99%) C.L.,

⁷The KARMEN experiment provides a tighter bound than the BUGEY experiment for $\delta m_{\text{LSND}}^2 > 0.2 \text{ eV}^2$, reaching $\frac{1}{4}A_{\text{SBL}}(\nu_\mu \rightarrow \nu_e) \sim 0.7 \times 10^{-3}$ at $\delta m_{\text{LSND}}^2 \sim 1 \text{ eV}^2$. However, atmospheric experiments average over the SBL contribution, and so are not sensitive to the value of δm_{LSND}^2 . Accordingly, the appropriate bound to use is the more liberal BUGEY bound, inferred at $\delta m_{\text{LSND}}^2 \sim 0.2 \text{ eV}^2$.

which translates into $|\epsilon_{\mu\mu}|^2 + |\epsilon_{\mu e}|^2 < 0.12$ (0.16). We note that the CHOOZ limit on ν_e -disappearance at the atmosphere scale is of order $(\epsilon_{\mu e}, \epsilon_{ee})^4 \lesssim 10^{-4}$ in the context of the 2+2 model, and so is not of interest.

To summarize these constraints, the 90% C.L. bounds which we will use in our numerical evaluation of the sum rules are: (i) $|\epsilon_{ee}|^2 + |\epsilon_{\mu e}|^2 \leq 0.01$, and (ii) $|\epsilon_{\mu\mu}|^2 < 0.12$. Note that these bounds allow ϵ_{ee} and $\epsilon_{\mu e}$ to be as large as 0.10, and allow $\epsilon_{\mu\mu}$ to be as large as 0.35.

Before ending this discussion of the SBL amplitudes, we note in passing a new product rule for SBL amplitudes. Emerging from eqs. (33)-(36) is

$$\left[\frac{P(\nu_e \rightarrow \nu_s)}{P(\nu_e \rightarrow \nu_\tau)} \right]_{\text{SBL}} \times \left[\frac{P(\nu_\mu \rightarrow \nu_s)}{P(\nu_\mu \rightarrow \nu_\tau)} \right]_{\text{SBL}} = 1, \quad (37)$$

exact to order ϵ^2 , at least.

Next we turn to the amplitudes for solar neutrino oscillations. We employ again the adiabatic approximation valid for large solar-mixing solutions, and simplify the discussion here with the $\nu_\odot \equiv \nu_2$ approximation. To $\mathcal{O}(\epsilon^2)$, the expansion of ν_2 in flavor states is

$$|\nu_2 \rangle = \begin{cases} (\epsilon_{\mu\mu} \cos \theta_{\text{sun}} - \epsilon_{\mu e} \sin \theta_{\text{sun}}) |\nu_\mu \rangle \\ + (\sin \theta_{\tau s} [\cos \theta_{\text{sun}} (1 - \frac{1}{2} |\epsilon_{\mu\mu}|^2) + \sin \theta_{\text{sun}} \epsilon_{\mu\mu}^* \epsilon_{\mu e}] - \cos \theta_{\tau s} \sin \theta_{\text{sun}} \epsilon_{ee}) |\nu_\tau \rangle \\ + (\cos \theta_{\tau s} [\cos \theta_{\text{sun}} (1 - \frac{1}{2} |\epsilon_{\mu\mu}|^2) + \sin \theta_{\text{sun}} \epsilon_{\mu\mu}^* \epsilon_{\mu e}] + \sin \theta_{\tau s} \sin \theta_{\text{sun}} \epsilon_{ee}) |\nu_s \rangle \\ - \sin \theta_{\text{sun}} (1 - \frac{1}{2} |\epsilon_{ee}|^2 - \frac{1}{2} |\epsilon_{\mu e}|^2) |\nu_e \rangle. \end{cases} \quad (38)$$

For solar neutrinos arriving at the “day” hemisphere of the earth, all angles assume vacuum values. This result generalizes eqn. (23) to nonzero ϵ 's. From this, one can easily calculate the first term in the sum rule (27),

$$\left[\frac{P(\nu_\odot \rightarrow \nu_s)}{P(\nu_\odot \rightarrow \nu_\tau)} \right]_{\text{sun}} \simeq \frac{|\langle \nu_s | \nu_2 \rangle|^2}{1 - |\langle \nu_e | \nu_2 \rangle|^2}, \quad (39)$$

as a function of the large and small angles. Similarly, the first factor in the product rule (28),

$$\left[\frac{P(\nu_\odot \rightarrow \nu_s)}{P(\nu_\odot \rightarrow \nu_\tau)} \right]_{\text{sun}} \simeq \frac{|\langle \nu_s | \nu_2 \rangle|^2}{|\langle \nu_\tau | \nu_2 \rangle|^2}, \quad (40)$$

can be readily calculated.

Finally, we turn to the oscillation amplitudes for the atmospheric neutrinos. The second terms in the sum and product rules, namely,

$$\left[\frac{P(\nu_\mu \rightarrow \nu_s)}{P(\nu_\mu \rightarrow \nu_\mu)} \right]_{\text{atm}} = \frac{P_{\text{LBL}}(\nu_\mu \rightarrow \nu_s) + P_{\text{SBL}}(\nu_\mu \rightarrow \nu_s)}{P_{\text{LBL}}(\nu_\mu \rightarrow \nu_\mu) + P_{\text{SBL}}(\nu_\mu \rightarrow \nu_\mu)}, \quad (41)$$

and

$$\left[\frac{P(\nu_\mu \rightarrow \nu_s)}{P(\nu_\mu \rightarrow \nu_\tau)} \right]_{\text{atm}} = \frac{P_{\text{LBL}}(\nu_\mu \rightarrow \nu_s) + P_{\text{SBL}}(\nu_\mu \rightarrow \nu_s)}{P_{\text{LBL}}(\nu_\mu \rightarrow \nu_\tau) + P_{\text{SBL}}(\nu_\mu \rightarrow \nu_\tau)}, \quad (42)$$

respectively, are given by inputting the appropriate amplitudes. In the atmospheric data, the measurement process averages over oscillation scales small relative to the Earth's radius. Hence it is correct and necessary to include contributions from the LBL length-scale and smaller, which here includes the oscillation-averaged short baseline amplitudes. One notes that the SBL amplitudes, given in eqs. (30)-(36), contribute to the sum rules at order ϵ^2 but not order ϵ . The long baseline amplitudes to order ϵ^2 are:

$$\begin{aligned} A_{\text{LBL}}(\nu_\mu \rightarrow \nu_s) &= \sin^2 2\theta_{\text{atm}} [\sin^2 \theta_{\tau s} (1 - |\epsilon_{\mu e}|^2 - |\epsilon_{ee}|^2) - |\epsilon_{\mu\mu}|^2] \\ &\quad - \sin 4\theta_{\text{atm}} \left[\frac{1}{2} \sin 2\theta_{\tau s} \text{Re}(\epsilon_{\mu\mu}) + \text{Re}(\epsilon_{\mu\mu}\epsilon_{\mu e}^*) \sin^2 \theta_{\tau s} \right] \end{aligned} \quad (43)$$

$$\begin{aligned} A_{\text{LBL}}(\nu_\mu \rightarrow \nu_\tau) &= \sin^2 2\theta_{\text{atm}} [\cos^2 \theta_{\tau s} (1 - |\epsilon_{\mu e}|^2 - |\epsilon_{ee}|^2) - |\epsilon_{\mu\mu}|^2] \\ &\quad + \sin 4\theta_{\text{atm}} \left[\frac{1}{2} \sin 2\theta_{\tau s} \text{Re}(\epsilon_{\mu\mu}) - \text{Re}(\epsilon_{\mu\mu}\epsilon_{\mu e}^*) \cos^2 \theta_{\tau s} \right] \end{aligned} \quad (44)$$

$$A_{\text{LBL}}(\nu_\mu \rightarrow \nu_e) = -\sin 2\theta_{\text{atm}} [(|\epsilon_{\mu e}|^2 - |\epsilon_{ee}|^2) \sin 2\theta_{\text{atm}} + 2\text{Re}(\epsilon_{\mu e}^* \epsilon_{ee}) \cos 2\theta_{\text{atm}}] \quad (45)$$

$$A_{\text{LBL}}(\nu_\mu \rightarrow \nu_\mu) = \sin^2 2\theta_{\text{atm}} [1 - 2|\epsilon_{\mu e}|^2 - 2|\epsilon_{\mu\mu}|^2] - 2\sin 4\theta_{\text{atm}} \text{Re}(\epsilon_{\mu\mu}\epsilon_{\mu e}^*) \quad (46)$$

With eqs. (39)-(42) as our guide, it is not difficult to write out the explicit analytic expressions for the sum and product rules. It is also not especially illuminating to do so. One finding is that the order ϵ and ϵ^2 corrections are different for the sum and product rules. Thus these two rules, containing the same information in zeroth order, contain different information when the small angles are included. We remind the reader that atmospheric oscillations occur in the earth, and so the mixing angles that enter eqs. (41) and (42) are matter rather than vacuum angles.

IV. MATTER EFFECTS

As has already been discussed, the effect of solar matter on the emerging solar neutrinos is very significant. Turning to earth-matter, we find in our numerical work that its effects

are small at low neutrino energies ~ 1 GeV, but large at high energies. Thus at low energy, the neutrino plots we show are little changed for the atmospheric antineutrino flux. Among the energy bins we consider, the largest difference for neutrino vs. antineutrino occurs in the 1.5 to 30 GeV bin. At still higher energies, we find the main effect of matter is a suppression of oscillation, common to both neutrinos and antineutrinos, and an interesting resonance at the δm^2 scale, in the $\nu_\mu - \nu_\tau$ channel [19]. This resonance is independent of the sign of the matter potential for large $E \delta A_{NC} / \delta m_{\text{atm}}^2$, and so it too is common to both neutrinos and antineutrinos. Thus, we find that overall the sum rule results we show for neutrinos are little altered for antineutrinos.

The relevant part of the neutrino Hamiltonian in the flavor basis is

$$H_F^\kappa = U_V \frac{M_V^2}{2E} U_V^\dagger + A_\kappa. \quad (47)$$

The matter-induced potentials are $A = \frac{1}{2} \sqrt{2} G_F \text{diag}(-N_n, -N_n, 0, 2N_e - N_n)$ in the $(\nu_\mu, \nu_\tau, \nu_s, \nu_e)$ flavor-basis; N_e and N_n are the electron and neutron densities. For antineutrinos, the sign of A is reversed. Since an overall phase is not measurable, it is useful to translate A by $+N_n \mathbf{1}$ and use the relative potentials $A = \sqrt{2} G_F \text{diag}(0, 0, \frac{1}{2} N_n, N_e)$. With $N_e \approx N_n$, which holds in the earth and in the sun, one has $A \equiv (0, 0, A_{NC}, A_{CC})$, with $A_{CC} = \sqrt{2} G_F N_e \approx 2A_{NC}$, as presented earlier. Numerically, $A_{CC} = 0.80 \times 10^{-13} (N_e / N_A \text{cm}^{-3})$ eV. Electron densities in the earth's mantle and core are $(N_e)_M \approx 1.6 N_A / \text{cm}^3$ and $(N_e)_C \approx 6 N_A / \text{cm}^3$.

Diagonalization of (47) to

$$H_{(\text{diag})}^\kappa = U_\kappa^\dagger H_F^\kappa U_\kappa \quad (48)$$

is done numerically in our work. It yields the mixing-matrix in matter (U_κ) and the mass-squared eigenvalues in matter (the diagonal elements of $H_{(\text{diag})}^\kappa$). The matter contribution to the Hamiltonian can significantly alter the masses and mixing angles, compared to their vacuum values.

Insight into the multi-resonance possibilities among four neutrino flavors may be found by using the approach of [19]. The idea is to find a neutrino basis such that the effective Hamiltonian matrix, including matter potentials, nearly decouples into a resonant 2×2 sub-block embedded in the rest. Decoupling may occur when $E \delta A$ is matched to just one

of a hierarchy of δm^2 values. A two-neutrino analysis may then be applied to the decoupled 2×2 sub-block.

Consider the 2×2 effective Hamiltonian (hermitian) matrix

$$H = \begin{pmatrix} h_{22} & h_{21} \\ h_{21}^* & h_{11} \end{pmatrix}. \quad (49)$$

The rotation angle which diagonalizes H is given by

$$\tan(2\theta_M) = \frac{2|h_{21}|}{h_{22} - h_{11}}. \quad (50)$$

The oscillation amplitude is $\sin^2(2\theta_M)$. The eigenvalue difference is

$$\delta h = \sqrt{(h_{22} - h_{11})^2 + 4|h_{21}|^2} = 2E\delta m_M^2, \quad (51)$$

where the second equality defines the effective mass-squared difference δm_M^2 in matter.

It often happens that the denominator $h_{22} - h_{11}$ varies from positive through zero to a large negative value as energy or matter density are varied. When this is so, θ_M varies from its vacuum value θ_V , through resonance and maximal mixing at $\pi/4$, ultimately to nearly $\pi/2$. The resonance with $\theta_M = \pi/4$ and maximal oscillation amplitude $\sin^2(2\theta_M) = 1$ occurs when $h_{22} = h_{11}$. The resonance width, defined by the half-maximum amplitude $\sin^2(2\theta_M) = \frac{1}{2}$, i.e. $\tan^2(2\theta_M) = 1$, is given by $|h_{22} - h_{11}| = 2|h_{21}|$.

For comparison purposes, it is useful to recall the exact two-flavor results. The oscillation amplitudes in matter and vacuum are related by

$$\sin^2(2\theta_M) = \frac{\sin^2(2\theta_V)}{\sin^2(2\theta_V) + \xi}, \quad (52)$$

where ξ is defined by

$$\xi \equiv \left(\cos(2\theta_V) - \frac{2E\delta A}{\delta m^2} \right)^2 = \cos^2(2\theta_V) \left(1 - \frac{E}{E_R} \right)^2, \quad (53)$$

Here, $\delta A = A_1 - A_2$ is the difference in matter potentials ordered *opposite* to the difference in vacuum mass-squares, δm^2 , and the resonant energy in the two-flavor system is

$$E_R = \frac{\delta m^2 \cos(2\theta_V)}{2\delta A} = 10 \cos(2\theta_V) \left(\frac{\delta m^2}{2 \times 10^{-3} \text{eV}} \right)^2 \left(\frac{10^{-13} \text{eV}}{\delta A} \right) \text{GeV}. \quad (54)$$

Mass-squared differences in vacuum and matter are related by

$$\delta m_M^2 = \delta m^2 \sqrt{\sin^2(2\theta_V) + \xi}. \quad (55)$$

The oscillation length is changed from its vacuum value $\lambda_V = 2.48 (E/\text{GeV})(\text{eV}^2/\delta m^2)$ km to

$$\lambda_M = \frac{\delta m^2}{\delta m_M^2} \lambda_V = \frac{\lambda_V}{\sqrt{\sin^2(2\theta_V) + \xi}}. \quad (56)$$

Note that in the two-flavor analysis, a near maximal vacuum angle forces the resonant energy toward zero (eq. (54), and further, necessarily implies suppression of the amplitude (eq. (52)) and contraction of the oscillation length (eq. (56)). The atmospheric vacuum mixing-angle is nearly maximal.

Note also the trend as the energy E is increased: ξ varies from $\cos^2(2\theta_V)$ at low energy, to zero at resonance, to a value increasing as E^2 above resonance. At the resonant energy, the oscillation amplitude $\sin^2 2\theta_M$ attains its maximum, unity, the mass-squared difference attains its minimum, $(\delta m_M^2)_R = \delta m^2 \sin(2\theta_V)$, and the oscillation length is $\lambda_R = \lambda_V / \sin(2\theta_V)$. For small vacuum angles, these changes are large. With large mixing angles, the changes are not dramatic; in addition, the resonant energy is very small and the resonance is broad. The sign of $\delta m^2 / \delta A$ determines whether the resonances occur in the neutrino or antineutrino channel. For $\theta_V \leq 45^\circ$ (the “light side”), the neutrino (anti-neutrino) channel is resonant for δA as defined and δm^2 of same (opposite) sign. Equivalently, resonant oscillations occur in the neutrino channel when E_R as defined in (54) is positive, and in the anti-neutrino channel when E_R as defined is negative. As can be seen from eq. (52), large E suppression of oscillations is the same for neutrino and antineutrino.

For neutrino energies well above the resonant value, the oscillation amplitude is suppressed as E^{-2} , and the oscillation length is contracted toward its energy-independent asymptotic value $\lambda_M = 2\pi/|\delta A|$. Numerically, this asymptotic oscillation length is $\lambda_M = 1.3 (10^{-13}\text{eV}/|\delta A|) \times 10^4$ km, which is of order of the Earth’s diameter D_\oplus for the values of A_{NC} in earth matter. Before approaching its asymptotic value, the oscillation length reaches a maximum value of $\lambda_{\text{max}} = 2\pi/|\delta A| \sin 2\theta_V$. Thus, with just two flavors the main effect of matter at large energy is to shorten oscillations relative to their vacuum values, but especially to suppress oscillations as θ_M is pushed toward its asymptotic value of $\pi/2$.

In contrast, with four flavors, the six rotations and additional matter potential greatly

enrich the matter-dependent oscillations. Diagonalizing the effective 2×2 sub-blocks gives results qualitatively different from diagonalizing an exact 2×2 matrix in a true flavor basis. We find, for example, that in the energy range $\delta m_{\text{atm}}^2/A_{NC} \ll E \ll \delta m_{\text{LSND}}^2/A_{NC}$ the atmospheric oscillation probability for both ν_μ and $\bar{\nu}_\mu$ may be significantly enhanced by matter, when the small vacuum angles satisfy certain relations. This surprising result is contrary to the suppression one expects from studying a pure two-flavor model. We reserve the detailed analysis of particular oscillation-channels for a future publication [23], since the focus of this (already long) paper is the sum rule, which involves ratios of oscillation channels.

V. RESULTS

A. Zeroth Order

We begin our presentation of results with a plot (Fig. 1) of the zeroth order sum rule, and the exclusion boxes that result when all small angles are set to zero [15]. The axes labels are

$$R_{\text{atm}} \equiv \left[\frac{P(\nu_\mu \rightarrow \nu_s)}{P(\nu_\mu \rightarrow \nu_\mu)} \right]_{\text{atm}} \quad (57)$$

and

$$R_{\text{sun}} \equiv \left[\frac{P(\nu_\odot \rightarrow \nu_s)}{P(\nu_\odot \rightarrow \nu_\ell)} \right]_{\text{sun}}. \quad (58)$$

The 90% exclusions are 0.17 for the sterile contribution to the atmospheric data, and 0.45 for the sterile contribution to the solar data. The 99% exclusions are 0.26 and 0.75, respectively. A similar value of $R_{\text{sun}} < 0.7$ at 3σ is given in [14]). We have checked that the effect of earth matter on the sum and product rules is negligible (less than 1%) when the small angles are zero. As a consequence, the zeroth order plot of Fig. 1 stands as a prediction for oscillation data over the entire relevant range of atmospheric neutrino energies, 0.5 GeV to 500 GeV, when small angles are neglected. In the context of eqs. (27) and (28), this means that the change in $\theta_{\tau s}$ due to earth-matter is negligible in the whole [0.5, 500] GeV energy region when ϵ 's are set to zero.

As one sees in Fig. 1, the overt sterile of the 2+2 sum rule conflicts with the sterile exclusion bounds coming from the solar and atmospheric data when the three small angles of the 2+2 model are neglected. The 99% exclusion box just touches the sum-rule line at a single point, where $\tan^2 \theta_{\tau s} = R_{\text{atm}}/R_{\text{sun}} = 0.26/0.75$, or $\theta_{\tau s} = 30^\circ$. The question arises whether inclusion of these small angles can sufficiently scatter the sum rule and weaken the exclusion boxes to make the 2+2 model viable. Re-calculating the exclusion boxes with nonzero small angles is a formidable task beyond the scope of this paper. We note, however, that a global fit with the largest of the small angles ($\epsilon_{\mu\mu}$ in our notation) included has been performed. The consequence is an expanded exclusion box for the value of $\cos^2 \theta_{\tau s} \cos^2 \epsilon_{\mu\mu}$ derived from atmospheric neutrinos. However this latter quantity is not directly related to R_{atm} for $\epsilon_{\mu\mu} \neq 0$, and so we continue to show just the restricted fit (ϵ 's = 0) in the figures to follow. Nevertheless, the trend is clear and expected: adding the small angles allows a larger sterile neutrino component in the global data.

B. All Orders

We next show that the sum rule is significantly broadened when small angles are included.

We display our numerical results, which include the effects of the nonzero small-angles and matter, in scatter plots in the plane labeled by the two terms of the sum rule or product rule. Each scatter point is determined by a random choice of the three small angles within their allowed regions, and a random choice of $\theta_{\tau s}$ within the interval $[0, \frac{\pi}{2}]$. In the numerical work, we use the full rotation matrices for the small angles, rather than the small- ϵ expansion presented earlier. We allow each ϵ to range over $-\epsilon_{\text{XB}} \leq \epsilon \leq \epsilon_{\text{XB}}$, where the set of ϵ_{XB} are the experimental bounds derived earlier in this paper (either 0.10 or 0.35). We remind the reader that we must include negative values of ϵ to (partially) atone for our neglect of the CP-violating phases independently associated with each ϵ . We do not take on the extra burden of calculating with complex ϵ 's, as this would double the number of small-angle parameters, from three to six. For the atmospheric data sample, we restrict ourselves to the angular bin that is most up-going ($-1 \leq \cos \theta_z \leq -0.8$). The most up-going bin is chosen because events in this bin have the longest baseline and so have enhanced oscillation probabilities, and the best experimental test of the sterile/active neutrino ratio in atmospheric data involves the

matter-effect.

We simulate the low-energy atmospheric data set by averaging the incident neutrino energy over a specific energy range, and by averaging the zenith angle over $-1 \leq \cos \theta_z \leq -0.8$, for each scatter point. Four specified energy ranges are chosen. They are 0.5 to 1.5 GeV, to simulate the contained events, 1.5 to 30 GeV, to simulate the partially contained events, 30 to 500 GeV, to simulate the full range of through-going events, and 50 to 150 GeV, to display the “typical” energy of through-going events. Each point displayed in the scatter plot is constructed as the mean value of 500 events, each a product of 50 randomly chosen energy values times 10 randomly chosen zenith-angle values. To judge the stability of this averaging, we repeated some trials with 500 energy values times 100 zenith-angle values. The results differed by less than 1%.

For the solar data, we average over the energy range 5 to 15 MeV, by choosing 50 random points within this range.

The following numerical values of the solar LMA ⁸ and atmospheric best fits [15] are taken as fixed:

$$\begin{aligned}
\delta m_{\text{sun}}^2 &= 3.7 \times 10^{-5} \text{ eV}^2 \\
\tan^2 \theta_{\text{sun}} &= 0.37 \quad (i.e. \theta_{\text{sun}} = 31^\circ) \\
\tan^2 \theta_{\text{atm}} &= 0.66 \quad (i.e. \theta_{\text{atm}} = 39^\circ) \\
\delta m_{\text{atm}}^2 &= 2.4 \times 10^{-3} \text{ eV}^2.
\end{aligned}
\tag{59}$$

The allowed range for δm_{LSND}^2 is 1 to 0.2 eV². However, neither the atmospheric nor the solar data are sensitive to the exact value of δm_{LSND}^2 , so this parameter does not enter our analysis. It is instructive to compare the vacuum oscillation lengths with the Earth’s diameter D_\oplus , for each of the fixed mass scales. For the solar scale, we have

$$\lambda_V(\delta m_{\text{sun}}^2) = 53 D_\oplus \left(\frac{E}{10 \text{ GeV}} \right) \left(\frac{3.7 \times 10^{-5} \text{ eV}^2}{\delta m_{\text{sun}}^2} \right); \tag{60}$$

for the atmospheric scale, we have

$$\lambda_V(\delta m_{\text{atm}}^2) = 0.81 D_\oplus \left(\frac{E}{10 \text{ GeV}} \right) \left(\frac{2.4 \times 10^{-3} \text{ eV}^2}{\delta m_{\text{atm}}^2} \right); \tag{61}$$

⁸After publication of the SNO NC data the LMA solution is selected at 99 % C.L. [24]

and for the short-baseline scale we have

$$\lambda_V(\delta m_{\text{LSND}}^2) = 2.0 \times 10^{-3} D_{\oplus} \left(\frac{E}{10\text{GeV}} \right) \left(\frac{\text{eV}^2}{\delta m_{\text{LSND}}^2} \right). \quad (62)$$

As explained in the previous section, in earth these oscillation lengths are expanded near a resonance, and become constant well above any resonance. Nevertheless, the inferences are that the solar scale barely contributes to atmospheric data, and then only at the lowest energies (\lesssim few GeV); the SBL scale is averaged in the atmospheric data until $E \sim \text{TeV}$; and the atmospheric scale is well-tuned to the size of the earth (which is why the dramatic zenith-angle dependence was so readily discovered), and so must be handled with care. In our numerical work this has been done. Fast oscillations (e.g. oscillations driven by δm_{LSND}^2) are averaged over by setting large relative phases in the oscillation probabilities to zero by hand. The description of this procedure is given in Appendix IX.

Scatter plots for the sum rule resulting from these central values are displayed in Figs. 2-5. The number of points in each scatter plot, and in each of those to follow, is 4,000. This number is chosen as a balance between computer time and the density of the final scatter plot. Also shown in these figures as a guide to the eye are the 90% and 99% exclusion boxes that result when all three small angles are set to zero. The weakening of the sum rule when small angles and matter effects are included in the oscillation physics is evident. At high energies, the sum rule has so relaxed that a large fraction of the allowed scatter points even lie within the allowed region of the conservative, zero ϵ , exclusion boxes.

To allow the reader to assess the relative significance of matter-effects in earth, we show the same plots with earth matter omitted in the bottom windows. It is seen that earth-matter effects are not significant at low energies but become important with increasing energy. Near a resonance, earth-matter will affect neutrinos and antineutrinos quite differently. Above a resonance, earth-matter will have the same effect on neutrinos and antineutrinos. Whenever earth-matter effects are evident, we have also run the same figure in the antineutrino channel to determine whether the matter-effect is different or the same for this channel. We discuss the antineutrino channel in section V E.

The earth-matter effects on the atmospheric ratio R_{atm} contributing to the sum rule (27) are evident, but still much less dramatic than the matter effects on individual atmospheric oscillation probabilities. In particular, the sum rule has some built-in stability against earth-

matter effects on the ν_μ oscillation. If the atmospheric oscillation were pure $\nu_\mu \rightarrow \nu_s$, then the atmospheric ratio appearing in (27) is one by definition, independent of any matter effects. If, at the other extreme, the atmospheric oscillation were pure $\nu_\mu \rightarrow \nu_\tau$, then the atmospheric ratio in (27) is zero by definition, again independent of any matter effects. The intermediate cases will show some intermediate but not large matter effect. The ratios defined for the sum rule tend to cancel individual variations in $P(\nu_\mu \rightarrow \nu_s)$ and $P(\nu_\mu \rightarrow \nu_\tau)$. In addition, the SBL contributions to the oscillation amplitudes, arising from the large δm_{LSND}^2 , are not matter suppressed, and so tend to stabilize the sum rule. One may expect matter effects to be more pronounced in the product rule (28), in that the stability argued here is less applicable for a product than for a sum, and less applicable for the ratios defined for the product rule compared to those of the sum rule.

One remarkable feature of Figs. 2 to 5 is the energy dependence of the sum rule. A roughly diagonal band in the plots at low energy ($\lesssim 30$ GeV) turns into a butterfly at high energy ($\gtrsim 30$ GeV). This is a result of the energy-dependent matter-effects on the oscillation amplitude and length, and of suppression occurring when oscillation lengths are large compared to the Earth's diameter.

While for low energies the zeroth order sum rule provides a good approximation to the 2+2 scheme with non-vanishing ϵ 's, i.e. $R_{\text{atm}} \sim \sin^2 \theta_{\tau s} \sim 1 - R_{\text{sun}}$, at high energies the dependence on $\theta_{\tau s}$ is quite different. This is explainable. At low energy the atmospheric oscillation is dominated by the LBL amplitude (43), leading to $R_{\text{atm}} \sim \sin^2 \theta_{\tau s}$. However, at high energy, the LBL amplitude is matter-suppressed at moderate to large $\theta_{\tau s}$ because then A_{NC} participates on the δm_{atm}^2 scale; while for small $\theta_{\tau s}$, the $\nu_\mu \rightarrow \nu_s$ oscillations occur dominantly via the matter-independent SBL scale, with amplitude given by $4 |\epsilon_{\mu\mu}|^2 \cos^2 \theta_{\tau s}$. We note the transition from $\sin^2 \theta_{\tau s}$ to $\cos^2 \theta_{\tau s}$ dominance as the energy grows from low to high. It is also possible that the changing oscillation length plays a role in the high-energy suppression of the LBL amplitude. As the energy increases, the wavelength grows first linearly with energy, then reaches a maximum and finally approaches its energy-independent asymptotic value. If the wavelength is long relative to the earth's diameter, then an experiment samples only a small fraction of a single oscillation cycle. For example, taking the vacuum oscillation length of $\lambda_V(\delta m_{\text{atm}}^2) \sim 10 D_\oplus (E_\nu/100\text{GeV})$ as a guide, one gets a sup-

pression of $\sin^2(\pi/10) = 0.1$ for $E_\nu \sim 100$ GeV; this may be compared to the SBL amplitude $4|\epsilon_{\mu\mu}|^2 \cos^2 \theta_{\tau s}$, which may be as large as 0.48. To summarize this discussion, the atmospheric oscillation at high energy is dominated by the SBL contribution (34) proportional to $\cos^2 \theta_{\tau s}$. Therefore, with $\theta_{\tau s} \sim \pi/2$, the sterile neutrino can hide from both the atmospheric through-going data and the solar data! For through-going events (E_ν above 30 GeV), the figures show that arbitrarily low sums seem possible. This may explain the good fits found for the pure $\nu_\mu \rightarrow \nu_s$ atmospheric model found in [15,25].

One moral to be drawn here is that the SuperK through-going (E_ν typically ~ 100 GeV) analysis with a single $\delta m^2 \sim 10^{-3} \text{eV}^2$ does not apply to the 2+2 model. With only a LBL contribution and no SBL contribution, R_{atm} is necessarily proportional to $\sin^2 \theta_{\tau s}$; then non-observation of ν_s -signatures will inevitably be interpreted as a small value for $\theta_{\tau s}$ and an absence of ν_s in the atmospheric sector of the theory.

We have analyzed the effects on the sum rule of variations in the solar and atmospheric mixing angles, and in the three δm^2 's. None of these variations had dramatic effects. The largest changes resulted from variations in δm_{sun}^2 and θ_{sun} , but especially in θ_{atm} . As the atmospheric angle decreases, the deviation from the sum rule increases.

C. Individual ϵ 's

An interesting question is what are the relative weights of each small angle in altering the sum rule result. To answer this, in Figs. 6 to 9 we present the dependence of the sum rule on the individual ϵ 's. A comparison shows that the effect of non-zero ϵ_{ee} on the sum rule is small, and that the strong deviations in the sum rule at high energies are induced by the non-vanishing $\epsilon_{\mu\mu}$ and $\epsilon_{\mu e}$. Especially interesting is the influence of $\epsilon_{\mu e}$, since this angle is set to zero in the global analyses of [15–17]. The results here suggest that at least the small mixing angles $\epsilon_{\mu\mu}$ and $\epsilon_{\mu e}$ must be consistently retained in the global analysis, and therefore casts some doubt on recent claimed exclusions of the 2+2 model.

D. Product Rule

In Fig. 10 we show the product rule for one selected energy range, $50 \text{ GeV} \leq E_\nu \leq 150 \text{ GeV}$. Here the axes labels are

$$R_{\text{atm}} \equiv \left[\frac{P(\nu_\mu \rightarrow \nu_s)}{P(\nu_\mu \rightarrow \nu_\tau)} \right]_{\text{atm}} \quad (63)$$

and

$$R_{\text{sun}} \equiv \left[\frac{P(\nu_\odot \rightarrow \nu_s)}{P(\nu_\odot \rightarrow \nu_\tau)} \right]_{\text{sun}} . \quad (64)$$

It is obvious that the deviation of the product rule from the diagonal line of the zeroth order result is even more pronounced than the deviation of the sum rule. We have argued in favor of this in an earlier section.

E. Atmospheric Antineutrinos

Oscillation probabilities for atmospheric antineutrinos are found by reversing the sign of the earth-matter potentials. When the ϵ 's are neglected, matter effects on the atmospheric ratios are negligible, and so the neutrino and antineutrino contributions to the sum rule are virtually identical. With nonzero ϵ 's, differences between antineutrino and neutrino may appear. Generally, we find that the antineutrino sum rule differs little from the neutrino sum rule, even with nonzero ϵ 's. None of the conclusions of this paper are affected by the small differences between atmospheric neutrino and antineutrino channels.

The largest difference in the sum rule occurs for the energy region 1.5 to 30 GeV, which contains matter resonances associated with the δm_{atm}^2 scale. In Fig. 11 we show the sum rule for the antineutrino channel in this energy region. This figure is to be compared to Fig. 3 for the neutrino channel. Larger differences between neutrino and antineutrino are found in the individual probabilities in this same energy region (not shown here). In the lower energy range 0.5 to 1.5 GeV, differences are not evident. At high energies above the resonance region ($\gtrsim 30 \text{ GeV}$), matter affects both channels nearly identically.

VI. SUMMARY AND CONCLUSIONS

In summary, we have investigated the validity of the sum rules (27) and (28) for the sterile neutrino, when the three small-angles in the general 4×4 mixing matrix are included, and when matter effects are included. To do so, we have reduced flavor-evolution calculations for solar and atmospheric neutrinos to numerical multiplication and diagonalization of 4×4 matrices. The inputs are the vacuum mixing matrix U_V , the vacuum mass-squared (or mass-squared difference) matrix M_V^2 , and the electron and neutron densities for the solar core, earth mantle, and earth core. The output from eq. (48) are the energy eigenvalues H^κ and mixing matrices U_κ , $\kappa = S, M, C$, in the solar core and earth mantle and core, respectively.

We find that the zeroth order sum rule offers a good approximation to the atmospheric data at low neutrino energies, but isn't valid at high energies. At high energies, the long-baseline amplitude is very matter-dependent, and the averaged short-baseline amplitude makes a significant contribution, even dominating for certain values of the mixing angles. Very small values for the corrected sum rule become possible. This means that the sterile neutrino of the 2+2 model can remain reasonably hidden from both solar and atmospheric neutrino oscillation data. We also find that both small angles $\epsilon_{\mu\mu}$ and $\epsilon_{\mu e}$ make significant contributions to amplitudes when matter effects are included. While $\epsilon_{\mu\mu}$ has been included in recent combined fits to solar and atmospheric neutrinos [15–17], the influence of a non-vanishing $\epsilon_{\mu e}$ has not yet been investigated. This weakens the case against the 2+2 model and the sterile neutrino.

We noted earlier that the important SBL amplitude, dominant in the atmospheric sector at high energies for some parameter range of the 2+2 model, is not included in the two angle, one δm^2 fits performed by SuperK. This seemingly invalidates any comparison of the SuperK analysis to the sterile neutrino of the 2+2 model.

Related but distinct from the sum rule is a product rule which we introduce. The product rule experiences even more pronounced deviations from zeroth order expectations due to non-vanishing ϵ 's and to matter. The variables of the product rule are more difficult to extract from data than are the variables of the sum rule.

VII. ACKNOWLEDGMENTS

We thank J. Conrad, A. de Gouvea, M.C. Gonzalez-Garcia, W.C. Louis, S. Parke, T. Schwetz, and A.Yu. Smirnov for useful discussions, and two of us (H. P. and T. J. W.) thank the Fermilab Summer Visitors Program for an environment that brought about completion of this work. This research was supported by U. S. Department of Energy grant number DE-FG05-85ER40226 and (HP) by the Bundesministerium für Bildung und Forschung (BMBF, Bonn Germany) under contract number 05HT1WWA2.

VIII. APPENDIX A: INCLUSION OF EARTH–MATTER EFFECTS

In this Appendix we discuss some details of the earth-matter effects, and their inclusion in our calculation of the sum rules.

A. Atmospheric Neutrinos

Neutrinos originating in the atmosphere traverse a chord of the earth before measurement. Neutrinos which emerge from the earth at zenith angle θ greater than 33° traverse just the mantle. Neutrinos which emerge from the earth at zenith angle less than 33° traverse the mantle, core, and more mantle, in a fashion nearly symmetric about the midpoint. We take the earth core to have near-constant density $N_e = N_n = 6 N_A/\text{cm}^3$ out to $R_C = 3493$ km, and the mantle to have near-constant density $N_e = N_n = 1.6 N_A/\text{cm}^3$ out to the Earth's surface at $R_\oplus = 6371$ km. When the mantle and core are approximated as constant-density layers, it is straightforward to write down an analytic solution for flavor propagation of atmospheric neutrinos through the earth.

To obtain the analytic solution, one notes that flavor states are continuous across matter discontinuities, whereas mass states propagate unmixed (i.e. diagonalize the Hamiltonian) within the constant-density layers. Thus, the analytic solution is a product of bases-changing matrices. Starting with an atmospheric ν_α , the final flavor state emerging from the earth is

$$\begin{aligned}
 |\nu_F(\theta)\rangle &= |\nu_\beta\rangle \langle \nu_\beta | \nu_l; M \rangle \langle \nu_l; M | e^{-iH_M r_M} | \nu_l; M \rangle \langle \nu_l; M | \nu_\gamma \rangle \langle \nu_\gamma | \nu_k; C \rangle \\
 &\times \langle \nu_k; C | e^{-2iH_C r_C} | \nu_k; C \rangle \langle \nu_k; C | \nu_\sigma \rangle \langle \nu_\sigma | \nu_j; M \rangle \\
 &\times \langle \nu_j; M | e^{-iH_M r_M} | \nu_j; M \rangle \langle \nu_j; M | \nu_\alpha \rangle .
 \end{aligned} \tag{65}$$

As usual, repeated indices are summed. Inputting eqs. (1) and (2) into (65), one gets

$$|\nu_F(\theta)\rangle = U_{\beta\alpha}^E(\theta) |\nu_\beta\rangle, \tag{66}$$

with the unitary evolution matrix for the Earth given by

$$U^E(\theta) = \left[U_M e^{-iH_M r_M} U_M^\dagger \right] \left[U_C e^{-2iH_C r_C} U_C^\dagger \right] \left[U_M e^{-iH_M r_M} U_M^\dagger \right]. \tag{67}$$

The propagation matrices $e^{-iH_\kappa r}$ are diagonal, with elements determined by replacing the Hamiltonian H_κ with its eigenvalues. These eigenvalues, and the mixing-matrices, are obtained by diagonalizing (numerically) the flavor-space Hamiltonian (47).

Any matrix proportional to the identity matrix may be subtracted from any of the H 's, since this just changes the unmeasurable overall phase of $|\nu_F\rangle$.

The θ dependence on the r.h.s. of eq. (67) is implicit in the values for the lengths r_M and r_C . For a neutrino direction with zenith angle $\theta < \sin^{-1}(R_C/R_\oplus) = 33^\circ$, half of the transit distance through the core is given by

$$r_C = \sqrt{R_C^2 - R_\oplus^2 \sin^2 \theta}, \quad (68)$$

and each of the two transits through the mantle has a length given by

$$r_M = R_\oplus \cos \theta - r_C. \quad (69)$$

For $\theta > 33^\circ$, the path is purely in the mantle, so $r_C = 0$ and the chord length is $2r_M = 2R_\oplus \cos \theta$.

For atmospheric neutrinos, we are especially interested in the probabilities

$$P_{\mu \rightarrow \beta} = |\langle \nu_\beta | U^E | \nu_\mu \rangle|^2 = |U_{\beta\mu}^E|^2 \quad (70)$$

and

$$P_{\mu \rightarrow \mu} = 1 - |\langle \nu_\mu | U^E | \nu_\mu \rangle|^2 = \sum_{\beta \neq \mu} |U_{\beta\mu}^E|^2. \quad (71)$$

We use this final equality as a check on our numerical work.

B. Solar Neutrinos, Day-Night Differences

For solar neutrinos arriving during the daytime, eq. (21) applies as it is. For neutrinos arriving at night, further flavor evolution (“ ν_e regeneration”) may occur in the earth-matter. The evolution equation (66) and its adjoint are used to calculate possible earth regeneration of the ν_e component in the solar neutrino flux. The density operator for the solar neutrino ensemble in the flavor basis is obtained from eq. (20) via the change of basis eq. (2) and its

adjoint in vacuum. Then, the flavor states are evolved according to eq. (66) and its adjoint. The result is a density matrix for the flavors emerging from the earth, given by

$$\rho_{[\text{flavor}]}^{S+E}(\theta) = U_E U_V D_S U_V^\dagger U_E^\dagger, \quad (72)$$

where the weights for the density matrix are contained in

$$D_S = \text{diag}(|U_{e4}^S|^2, \dots, |U_{e1}^S|^2). \quad (73)$$

The final result of interest is

$$P^{S+E}(\nu_e \rightarrow \nu\beta) = (\rho_{[\text{flavor}]}^{S+E})_{\beta\beta}. \quad (74)$$

In our numerical work, we do not pursue earth regeneration of solar neutrinos because the effect is known to be small. In addition, the effect is not present in the daytime data.

IX. APPENDIX B: IMPLEMENTING L/E RESOLUTION

Experimental reconstruction of the neutrino energy E and pathlength L is limited by information loss when the neutrino undergoes CC scattering, and by experimental resolution. Such smearing in the data averages out the interferences among the shorter-wavelength oscillations. Also, transit of path lengths much longer than the oscillation length leads to decoherence of the mass-eigenstate wave packets, again removing the interference terms. We may implement interference loss or averaging as follows:

For $\theta < 33^\circ$, one has, from eq. (70), via eqs. (65) and (67),

$$P_{\mu \rightarrow \beta} = e^{-i\Phi(l,k,j;s,q,p)} U_{M;\beta l} U_{MC;lk} U_{MC;kj}^\dagger U_{M;j\mu}^\dagger U_{M;\mu p} U_{MC;pq} U_{MC;qs}^\dagger U_{M;s\beta}^\dagger; \quad (75)$$

where $U_{MC} = U_M^\dagger U_C$, there is no sum on β and μ , and the phase governing the interferences is

$$\begin{aligned} \Phi(l, k, j; s, q, p) &= \phi(l; s) + \phi(k; q) + \phi(j; p) \\ &= (H_l^M - H_s^M) r_M + (H_k^C - H_q^C) (2r_C) + (H_j^M - H_p^M) r_M. \end{aligned} \quad (76)$$

For $\theta > 33^\circ$, the result is much simpler:

$$P_{\mu \rightarrow \beta} = e^{-i\Phi(j;p)} U_{M;\beta j} U_{M;j\mu}^\dagger U_{M;\mu p} U_{M;p\beta}^\dagger ; \quad (77)$$

again with no sum on β and μ , and the phase given by

$$\Phi(j;p) = (H_j^M - H_p^M) (2R_\oplus \cos \theta) . \quad (78)$$

If the experimental resolution and/or reconstruction of neutrino L/E is $n\%$, then a phase in excess of $\sim \frac{100}{n} \pi$ will be smeared sufficiently that $e^{-i\Phi}$ effectively averages to zero. Thus in numerical work, one may set to zero contributions from values of $\{l, k, j; s, q, p\}$ in eq. (76) and $\{j; p\}$ in eq. (78) yielding a phase in excess of, say, 10π . In this way, all sub-dominant as well as dominant contributions to the oscillation result are included. In particular, phases proportional to the LSND mass-gap may be safely set to zero.

In our work, we explicitly set the phases proportional to the LSND mass-gap to zero. The other phases, proportional to δm_{atm}^2 or δm_{sun}^2 , are kept, but averaged over 50 energies and 10 zenith angles, as explained in the main text.

X. APPENDIX C: ATMOSPHERIC DENSITY MATRIX

One may go beyond the evolution of just the single atmospheric flavor ν_μ . An atmospheric density operator will characterize the incoherent flavor mixture produced in the atmosphere. For example, taking the flavor content of neutrinos from pion decay, one has

$$\hat{\rho}_{[\text{flavor}]}^A = \frac{2}{3} |\nu_\mu \rangle \langle \nu_\mu| + \frac{1}{3} |\nu_e \rangle \langle \nu_e| . \quad (79)$$

The final density matrix is given by

$$\rho_{[\text{flavor}]}^{A+E}(\theta) = U_E D_A U_E^\dagger , \quad (80)$$

with weight matrix $D_A = \text{diag}(\frac{2}{3}, 0, 0, \frac{1}{3})$. The final probabilities are

$$P^{A+E} \nu_A \rightarrow \nu_\beta = \left(\rho_{[\text{flavor}]}^{A+E} \right)_{\beta\beta} . \quad (81)$$

We do not pursue this subtlety in the text.

REFERENCES

- [1] miniBooNE homepage: <http://www-boone.fnal.gov>
- [2] S. M. Bilenkii, C. Giunti and W. Grimus, *Eur. Phys. J. C* **1**, 247 (1998) [arXiv:hep-ph/9607372].
- [3] V. Barger, S. Pakvasa, T. J. Weiler and K. Whisnant, *Phys. Rev. D* **58**, 093016 (1998) [hep-ph/9806328].
- [4] G. B. Mills [LSND Collaboration], *Nucl. Phys. Proc. Suppl.* **91**, 198 (2001).
- [5] V. Barger, B. Kayser, J. Learned, T. Weiler and K. Whisnant, *Phys. Lett. B* **489**, 345 (2000) [hep-ph/0008019].
- [6] A. Y. Smirnov, *Nucl. Phys. Proc. Suppl.* **91**, 306 (2000) [hep-ph/0010097].
- [7] C. Giunti and M. Laveder, *JHEP***0102**, 001 (2001) [hep-ph/0010009].
- [8] W. Grimus and T. Schwetz, *Eur. Phys. J. C* **20**, 1 (2001) [arXiv:hep-ph/0102252].
- [9] O. L. Peres and A. Y. Smirnov, *Nucl. Phys. B* **599**, 3 (2001) [hep-ph/0011054].
- [10] A. Habig [SuperKamiokande Collaboration], arXiv:hep-ex/0106025; M. Shiozawa (SuperK Collaboration), presented at “Neutrino2002,” Munich, Germany, May 2002.
- [11] G. Fogli, E. Lisi, and A. Marrone, *Phys. Rev. D* **63**, 053008 (2001).
- [12] C. Giunti, M. C. Gonzalez-Garcia and C. Peña-Garay, *Phys. Rev. D* **62**, 013005 (2000) [arXiv:hep-ph/0001101].
- [13] V. D. Barger, D. Marfatia and K. Whisnant, arXiv:hep-ph/0106207.
- [14] J. N. Bahcall, M. C. Gonzalez-Garcia and C. Peña-Garay, arXiv:hep-ph/0204314, V. Barger, D. Marfatia, K. Whisnant and B. P. Wood, arXiv:hep-ph/0204253, J. N. Bahcall, M. C. Gonzalez-Garcia and C. Peña-Garay, arXiv:hep-ph/0204194; A. Bandyopadhyay, S. Choubey, S. Goswami, and D.P. Roy, *Phys. Lett. B* **540**, 14 (2002).
- [15] M. C. Gonzalez-Garcia, M. Maltoni and C. Peña-Garay, *Phys. Rev. D* **64**, 093001

- (2001) [arXiv:hep-ph/0105269]. M. C. Gonzalez-Garcia, M. Maltoni and C. Peña-Garay, arXiv:hep-ph/0108073.
- [16] M. Maltoni, T. Schwetz and J. W. Valle, arXiv:hep-ph/0112103.
- [17] M. Maltoni, T. Schwetz, M. A. Tortola, and J. W. Valle, arXiv:hep-ph/0207157 and hep-ph/0207227.
- [18] M. Gronau, R. Johnson and J. Schechter, Phys. Rev. D **32**, 3062 (1985).
- [19] D. Dooling, C. Giunti, K. Kang and C. W. Kim, Phys. Rev. D **61**, 073011 (2000) [arXiv:hep-ph/9908513]; also, [11] for the zero ϵ analysis; these works extends the much earlier three-neutrino work of T. K. Kuo and J. Pantaleone, Phys. Rev. D **35**, 3432 (1987).
- [20] <http://www.sno.phy.queensu.ca/>
- [21] Y. Declais *et al.*, Nucl. Phys. B **434**, 503 (1995).
- [22] F. Dydak *et al.*, Phys. Lett. B **134**, 281 (1984).
- [23] H. Päs, L. Song, and T.J. Weiler, in preparation.
- [24] P. C. de Holanda and A. Y. Smirnov, arXiv:hep-ph/0205241, A. Strumia, C. Cattadori, N. Ferrari and F. Vissani, arXiv:hep-ph/0205261, A. Bandyopadhyay, S. Choubey, S. Goswami and D. P. Roy, arXiv:hep-ph/0204286.
- [25] R. Foot, Phys. Lett. B **496**, 169 (2000); *ibid*, arXiv:hep-ph/0210393; R. Foot and R. Volkas, Phys. Lett. B **543**, 38 (2002).

FIGURES

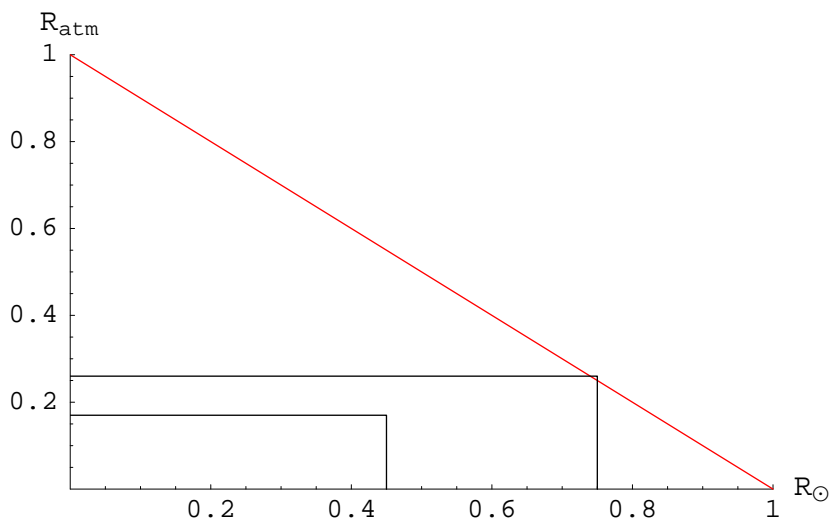


FIG. 1. The zeroth order sum rule compared to the 90% and 99% exclusion boxes obtained from fits to data with small angles set to zero. The vertical axis is R_{atm} and the horizontal axis is R_{sun} .

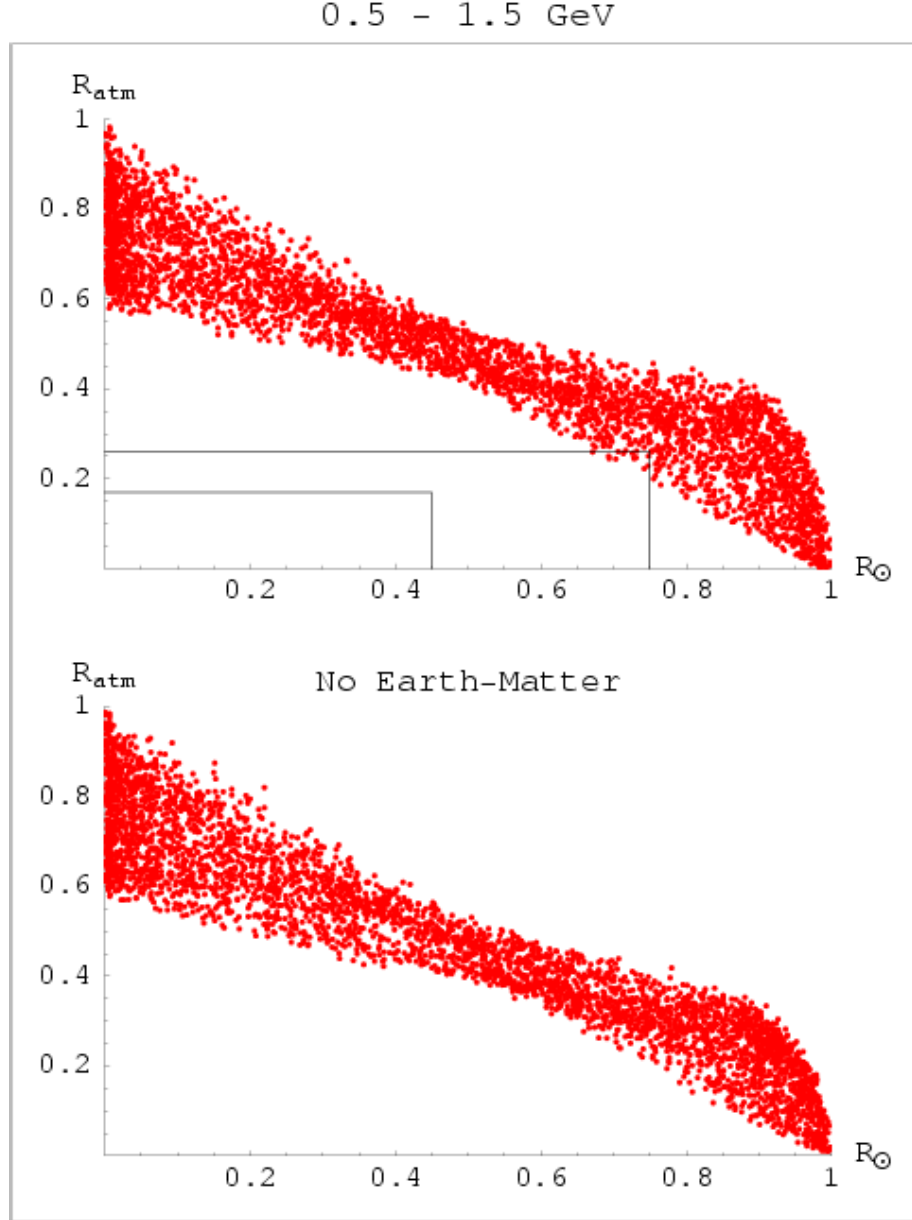


FIG. 2. Top: 4,000 points, each averaged over incident neutrino energies $0.5 \text{ GeV} \leq E_\nu \leq 1.5 \text{ GeV}$ and upcoming angles in $-1.0 \leq \cos \theta_z \leq -0.8$, scattered over $\epsilon_{\mu\mu}$, $\epsilon_{\mu e}$, ϵ_{ee} , and $\theta_{\tau s}$, with matter effects included. The 90% and 99% exclusion boxes obtained with small angles set to zero are shown as a crude reference. Bottom: same as above but with earth-matter omitted. In both plots, the vertical axis is R_{atm} and the horizontal axis is R_{sun} .

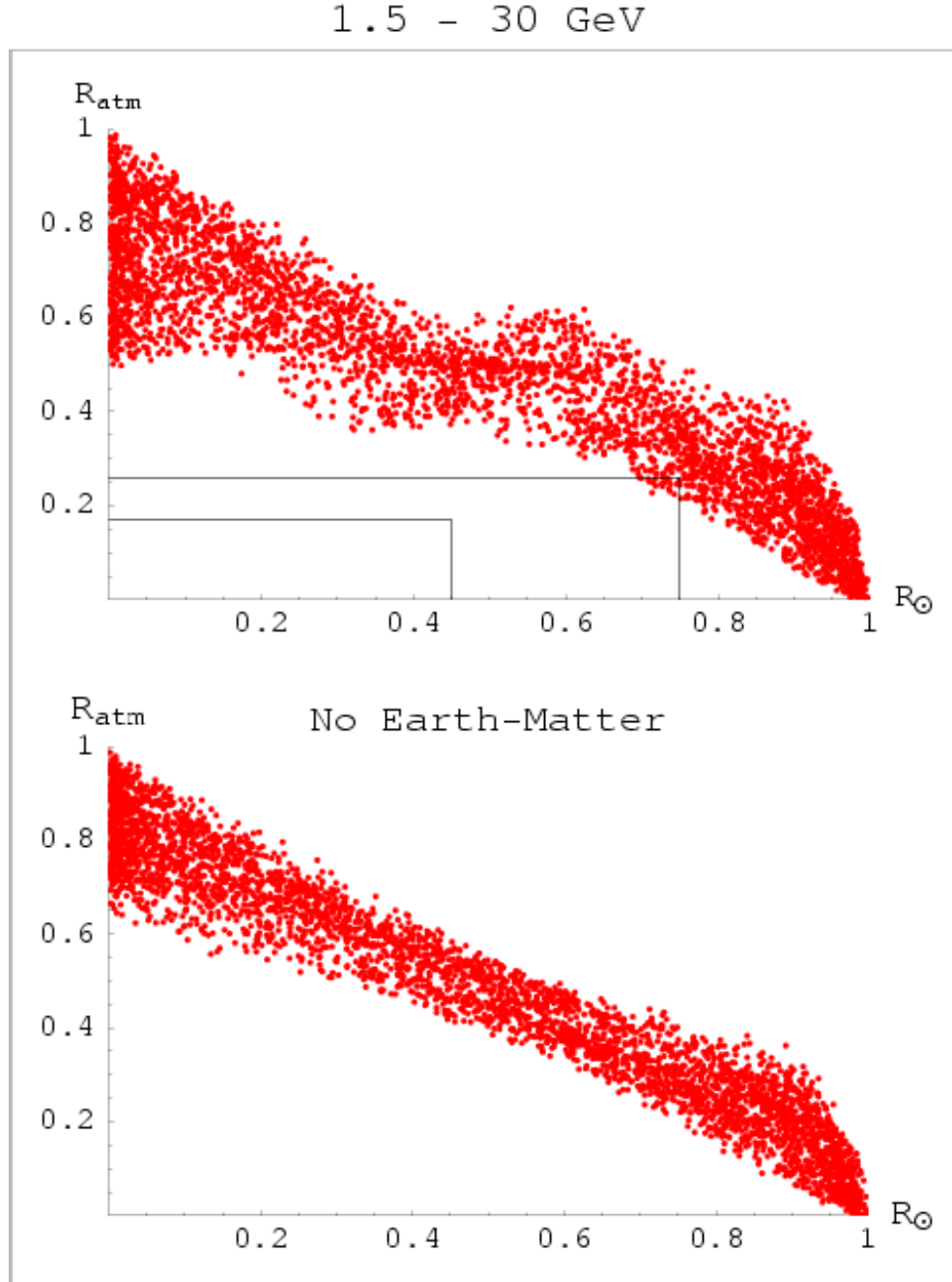


FIG. 3. Same as Fig. 2, but energy-averaged over $1.5 \text{ GeV} \leq E_{\nu} \leq 30 \text{ GeV}$.

30 - 500 GeV

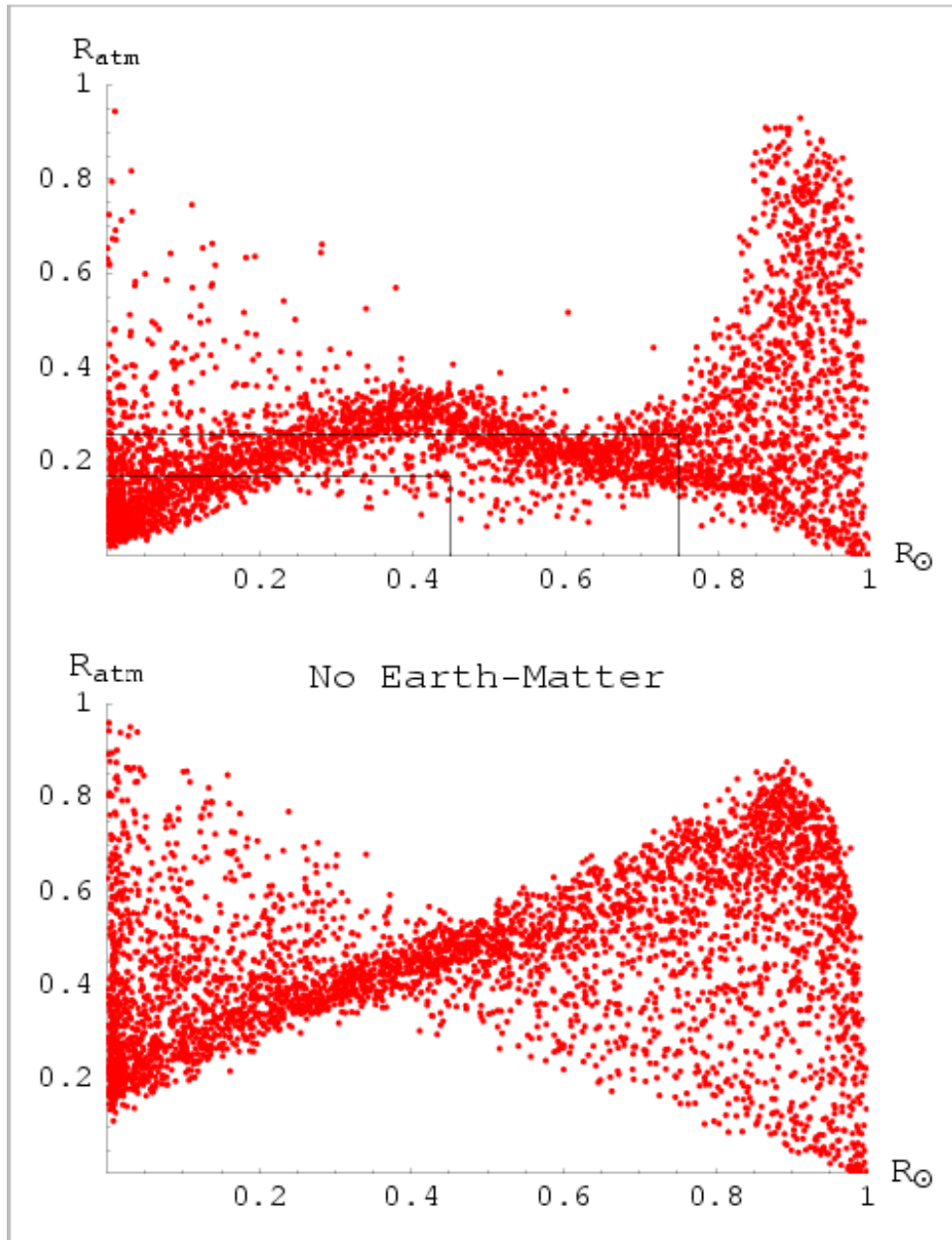


FIG. 4. Same as Fig. 2, but energy-averaged over $30 \text{ GeV} \leq E_{\nu} \leq 500 \text{ GeV}$.

50 - 150 GeV

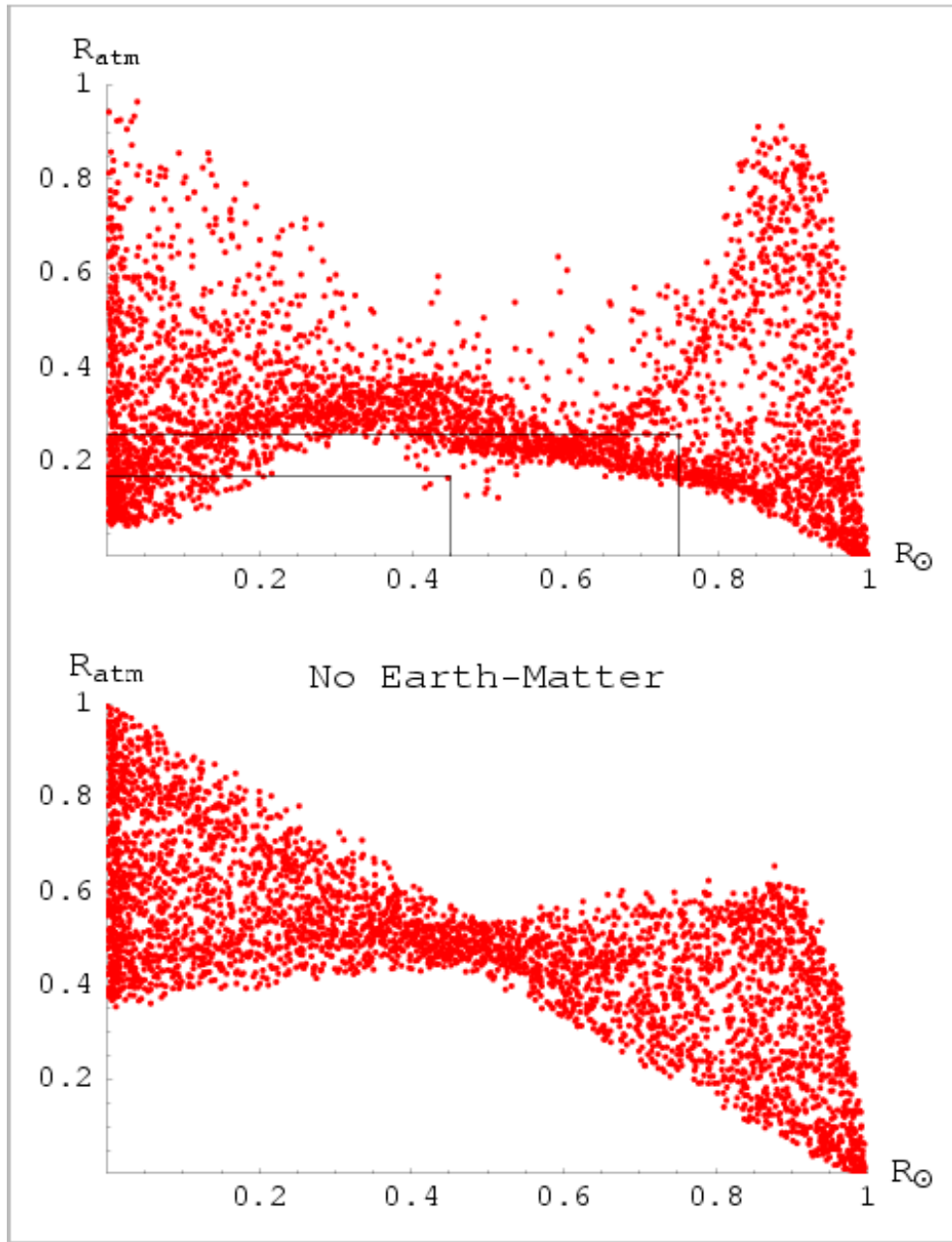


FIG. 5. Same as Fig. 2, but energy-averaged over $50 \text{ GeV} \leq E_{\nu} \leq 150 \text{ GeV}$.

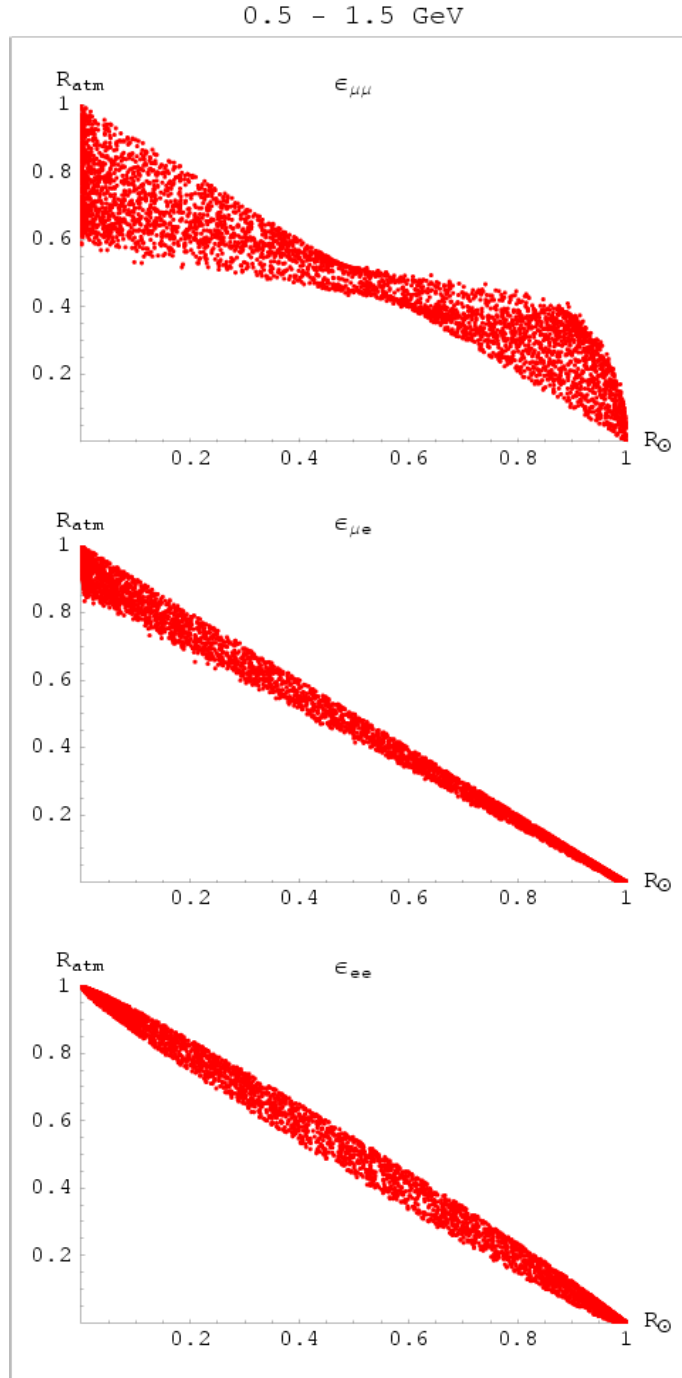


FIG. 6. Same as in Top figure 2, but with only one small-angle (indicated) nonzero.

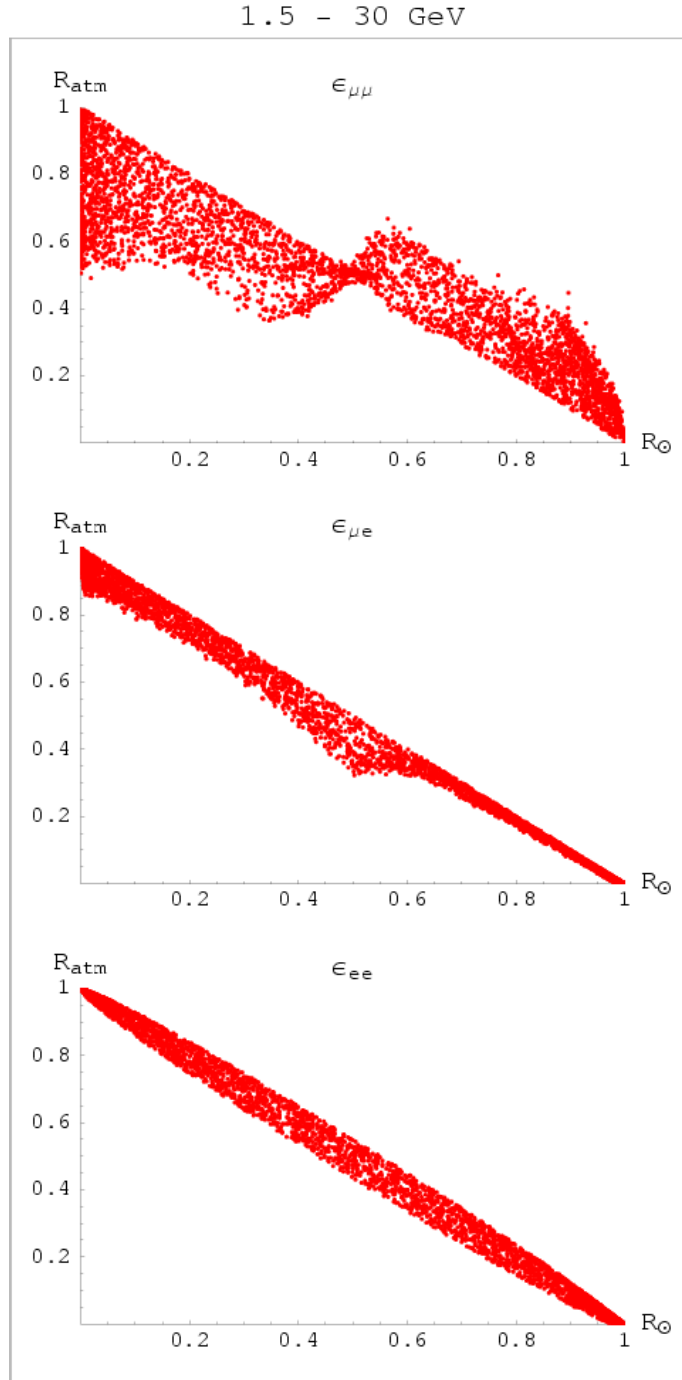


FIG. 7. Same as in Top figure 3, but with only one small-angle (indicated) nonzero.

30 - 500 GeV

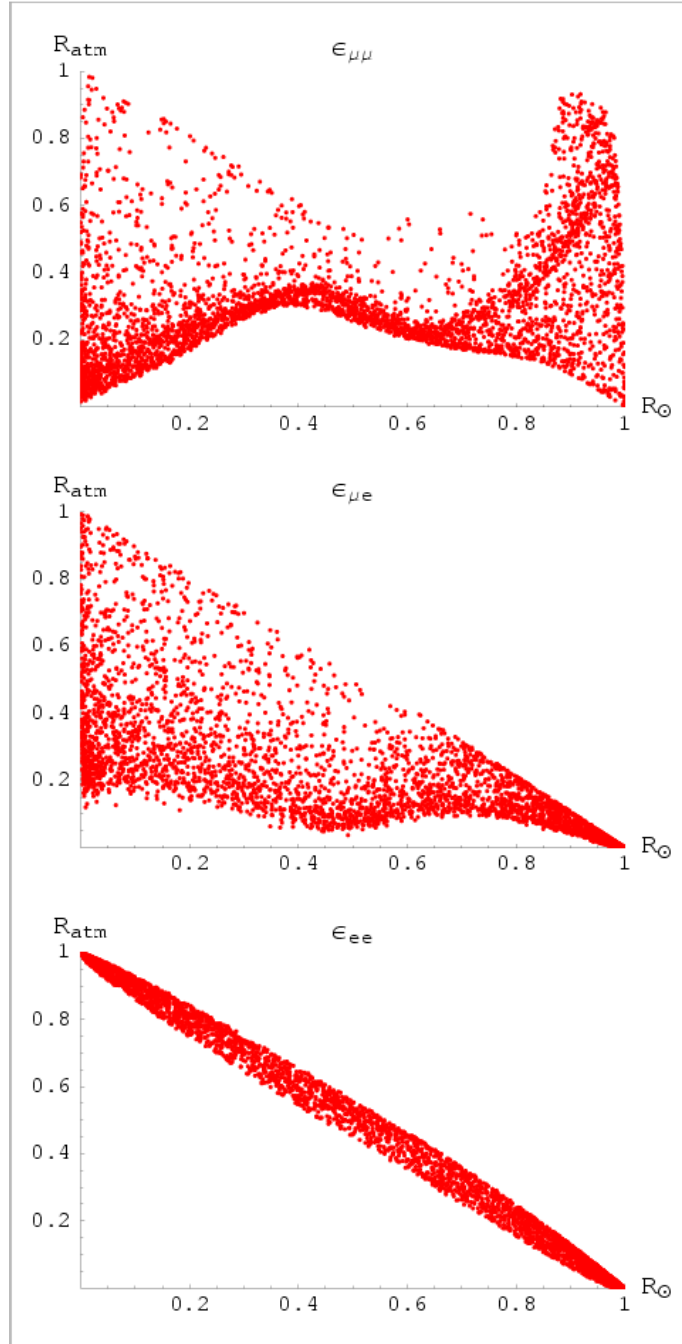


FIG. 8. Same as in Top figure 4, but with only one small-angle (indicated) nonzero.

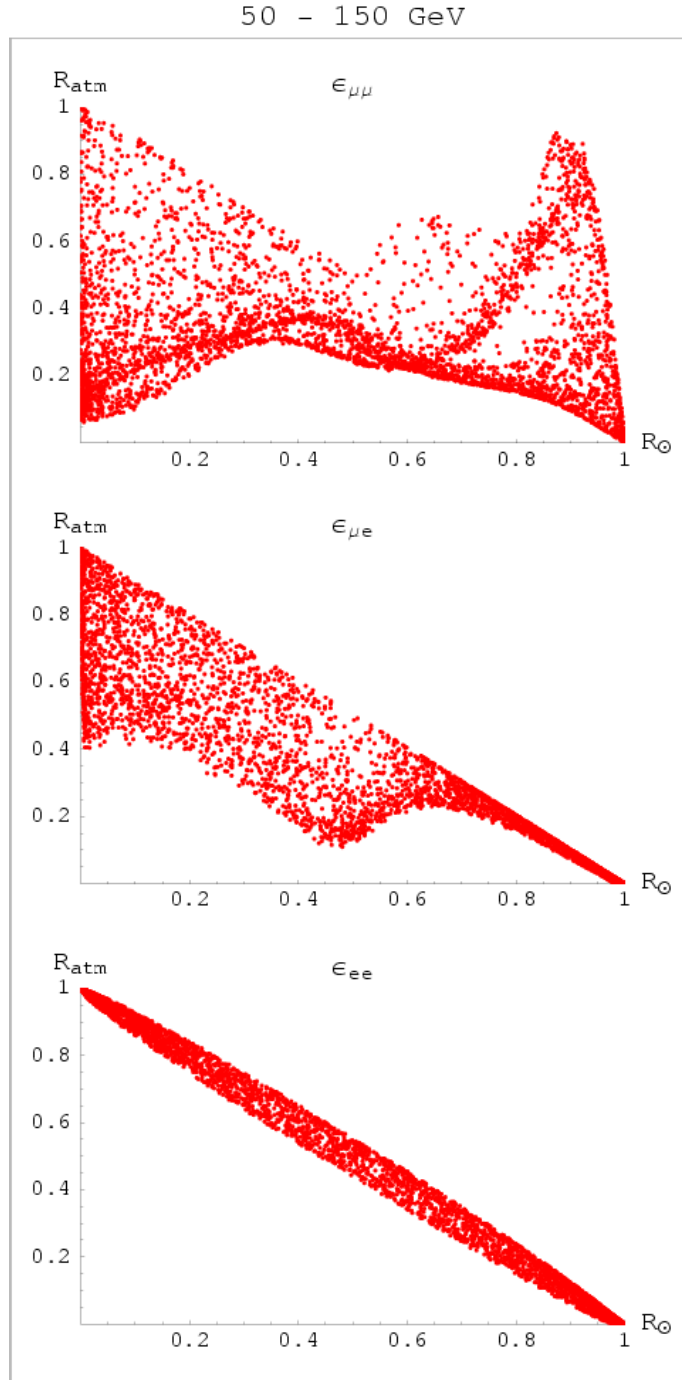


FIG. 9. Same as in Top figure 5, but with only one small-angle (indicated) nonzero.

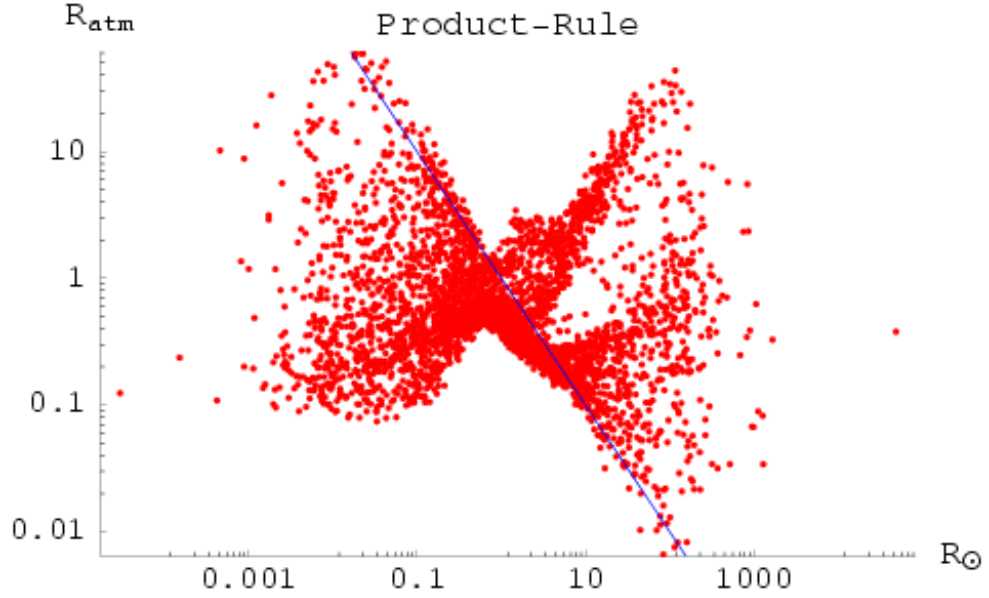


FIG. 10. 4,000 points for the product rule, each averaged over incident neutrino energies $50 \text{ GeV} \leq E_\nu \leq 150 \text{ GeV}$ and upcoming angles in $-1.0 \leq \cos\theta_z \leq -0.8$, scattered over $\epsilon_{\mu\mu}$, $\epsilon_{\mu e}$, ϵ_{ee} , and $\theta_{\tau s}$, with matter effects included. Here we use the same R_{atm} and R_{sun} symbols to denote the ratios of amplitudes appearing in the product rule eq. (28). The diagonal line is the result when small angles are set to zero.

1.5 - 30 GeV $\bar{\nu}$

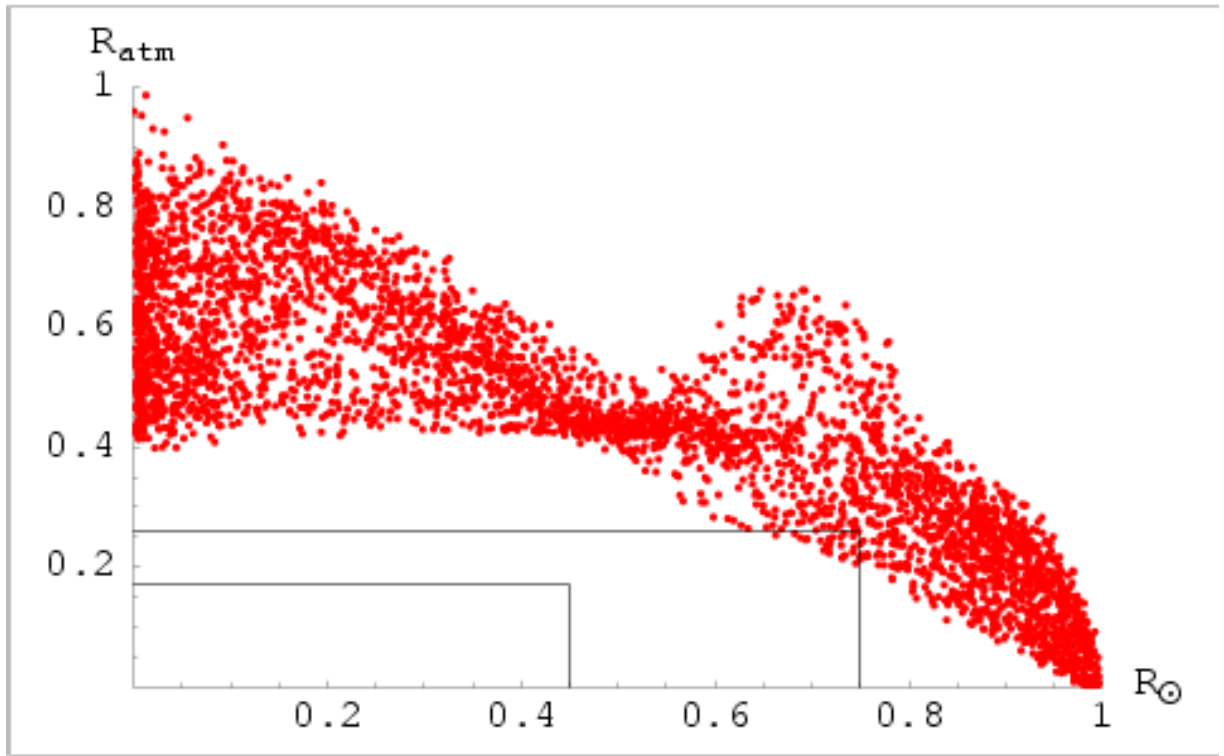


FIG. 11. Sum rule scatter plot for the antineutrino channel, averaged over the energy range 1.5 to 30 GeV.